





Multi-robot Relative Pose Estimation and IMU Preintegration Using Passive UWB Transceivers

Mohammed Ayman Shalaby , *Graduate Student Member, IEEE*, Charles Champagne Cossette , *Member, IEEE*, Jerome Le Ny , *Senior Member, IEEE*, and James Richard Forbes , *Member, IEEE*

Abstract—Ultra-wideband (UWB) systems are becoming increasingly popular as a means of inter-robot ranging and communication. A major constraint associated with UWB is that only one pair of UWB transceivers can range at a time to avoid interference, hence hindering the scalability of UWB-based localization. In this article, a ranging protocol is proposed that allows all robots to passively listen on neighboring communicating robots without any hierarchical restrictions on the role of the robots. This is utilized to allow each robot to obtain more range measurements and to broadcast preintegrated inertial measurement unit (IMU) measurements for relative extended pose state estimation directly on $SE_2(3)$. Consequently, a simultaneous clock-synchronization and relative-pose estimator is formulated using an on-manifold extended Kalman filter (EKF) and is evaluated in simulation using Monte Carlo runs for up to seven robots. The ranging protocol is implemented in C on custom-made UWB boards fitted to three quadcopters, and the proposed filter is evaluated over multiple experimental trials, yielding up to 48% improvement in localization accuracy.

Index Terms—Inertial measurement unit (IMU) preintegration, localization, multi-robot systems, range sensing.

I. INTRODUCTION

MULTI-ROBOT teams' prevalence is a direct consequence of two factors, recent advancements in available technology and demand for automating complex tasks. The former has recently been accelerated through the adoption of *ultra-wideband* (UWB) radio frequency signals as a means of *ranging* and communication between robots, where ranging means obtaining distance measurements. UWB is a relatively inexpensive, low-power, lightweight, and compact technology, which allows for high-rate ranging and data transfer. An example of UWB boards fitted to a quadcopter is shown in Fig. 1. Robotic teams

Manuscript received 16 October 2023; accepted 22 January 2024. Date of publication 27 February 2024; date of current version 8 April 2024. This paper was recommended for publication by Associate Editor G. Huang and Editor P. R. Giordano upon evaluation of the reviewers' comments. This work was supported in part by the NSERC Alliance Grant program, in part by the NSERC Discovery Grant program, in part by the CFI JELF program, and in part by the FRQNT Award under Grant 2018-PR-253646. (*Corresponding author: Mohammed Ayman Shalaby.*)

Mohammed Ayman Shalaby, Charles Champagne Cossette, and James Richard Forbes are with the Department of Mechanical Engineering, McGill University, Montreal, QC H3A 0C3, Canada (e-mail: mohammed.shalaby@mail.mcgill.ca; charles.cossette@mail.mcgill.ca; james.richard.forbes@mcgill.ca).

Jerome Le Ny is with the Department of Electrical Engineering, Polytechnique Montreal, Montreal, QC H3T 1J4, Canada (e-mail: jerome.le-ny@polymtl.ca).

This article has supplementary downloadable material available at <https://doi.org/10.1109/TRO.2024.3370027>, provided by the authors.

Digital Object Identifier 10.1109/TRO.2024.3370027

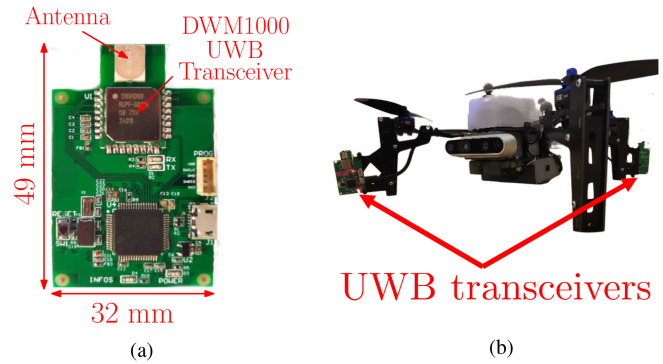


Fig. 1. Experimental setup. (a) Custom-made board fitted with a DWM1000 UWB transceiver. (b) Uvify IFO-S quadcopter equipped with two UWB transceivers 45 cm apart.

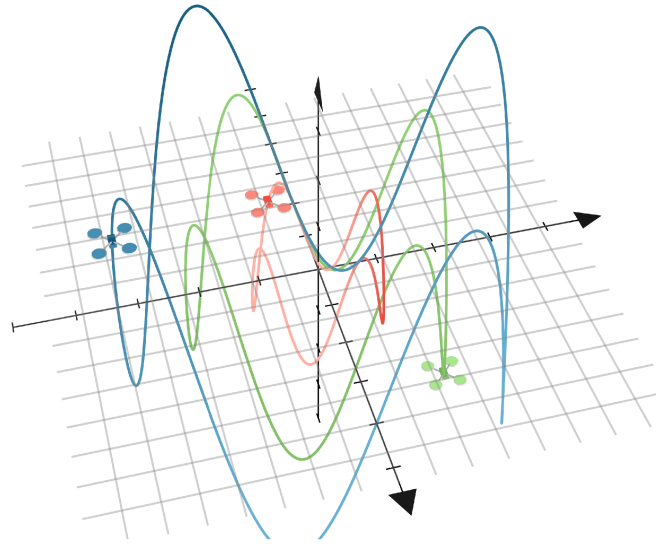


Fig. 2. Trajectories followed by three simulated quadcopters.

equipped with UWB and other sensors, such as cameras and/or *inertial measurement units* (IMUs), have been considered for relative pose estimation, which is a prerequisite for applications such as collision avoidance and collaborative mapping and infrastructure inspection.

Nonetheless, using UWB for relative pose estimation in multi-robot teams introduces a distinct set of problems. First, UWB ranging and communication is not robust to interference, thus imposing the constraint that only one pair of transceivers can

communicate at a time. This is typically addressed using *time-division multiple-access (TDMA)* media-access control (MAC) protocols alongside a round robin approach to determine which pair communicates at each time. However, the larger the team of robots, the longer the time gaps in between a robot ranging with another. Another complication with UWB ranging is the reliance on *time-of-flight (ToF)* measurements, which necessitates the presence of a clock at each UWB transceiver. However, in practice these clocks run at different rates, and therefore require some synchronization mechanism. The importance of synchronization can be highlighted by the fact that 1 ns in synchronization error translates to $c \text{ [m/s]} \times 10^{-9} \text{ [s]} \approx 30 \text{ [cm]}$ in localization error, where c is the speed of light.

Another practical issue associated with multirobot systems is communication constraints, which limit the amount of information that can be transmitted between robots. In filtering applications where there are, for example, three quadcopters moving randomly in a 3-D space, as shown in Fig. 2, IMU measurements must be broadcasted if robots are to estimate their neighbors' relative states directly from the raw measurements. Nonetheless, IMU measurements are typically recorded at a very high frequency, and the constraint that only one pair can be communicating at a time means that communication links between robots do not always exist. Therefore, a more efficient way of sharing odometry information is required.

To achieve a practical relative pose estimation solution that is implementable on a robotic team, this article addresses the aforementioned constraints. The contributions of this work are summarized as follows.

- 1) A ranging protocol is introduced that extends classical ranging protocols by allowing neighboring robots to passively listen to the measurements and timestamp receptions, with no assumptions or imposed constraints on the robots' hierarchy. The concept of passive listening is utilized to provide a $(1 + 3n)$ -fold increase in the number of measurements recorded when there are a total of $n + 1$ robots each equipped with two UWB transceivers. The concept of passive listening is additionally utilized for more efficient information sharing and implementing simple MAC protocols.
- 2) Representing the extended pose state as an element of $SE_2(3)$, an on-manifold tightly coupled simultaneous clock-synchronization and relative-pose estimator (CSRPE) is then proposed, which allows incorporating passive listening measurements in an extended Kalman filter (EKF) to improve the relative pose estimation. This provides a means for many different robots to estimate the relative poses of their neighbors relative to themselves at a high frequency.
- 3) Rather than sharing high-frequency IMU readings with neighbors, the concept of preintegration [1] is developed for relative pose states on $SE_2(3)$, and is used as a means of efficient IMU data logging and communication between robots. This is additionally incorporated in the CSRPE, where the theory behind filtering with delayed inputs is developed as the preintegrated IMU measurements arrive asynchronously from neighboring robots.

- 4) The proposed algorithm is evaluated in simulation using Monte Carlo trials and in experiments using four trials with three quadcopters equipped with two UWB transceivers each. It is shown that localization accuracy improves up to 23% when compared with a centralized scenario and up to 48% when compared with the case of no passive listening.

The remainder of this article is organized as follows. Related work is presented in Section II, and Lie group and UWB preliminaries are discussed in Section III. The problem is formulated in Section IV, then the proposed ranging protocol is discussed in Section V. The relative pose process model and preintegration on $SE_2(3)$ are discussed in Sections VI and VII, respectively. Simulation and experimental results are discussed in Sections VIII and IX, respectively, before further practical considerations are mentioned in Section X. Finally, Section XI concludes this article.

II. RELATED WORK

The majority of UWB-based localization relies on a set of prelocalized and synchronized static transceivers, or *anchors*, to localize a mobile transceiver [2], [3], [4]. This typically relies on the anchors ranging with the mobile transceiver using standard ranging protocols, such as *two-way ranging (TWR)* or *time-difference-of-arrival* [5], [6], [7, Ch. 7.1.4]. More complicated ranging protocols have been proposed in [8], [9], and [10] to allow multiple anchors to passively listen in on messages with the mobile transceiver to localize it.

Calibrating the clocks and location of anchors is challenging, and the Authors in [11] and [12] propose an approach where anchors actively range with one another to synchronize and localize themselves. Meanwhile, a mobile transceiver passively listens to these signals to localize itself using the anchors' estimated clock states and positions. The work in [13] and [14] extends this by applying a Kalman filter to the synchronization and localization problem. Meanwhile, in [15], the synchronization approach is accurate to within a few microseconds, whereas nanosecond-level accuracy is desired for localization with cm accuracy.

Overcoming the need for a fixed infrastructure of anchors, UWB has been used more recently for teams of robots [16], [17], [18]. In [19], it is assumed that neighboring robots know their poses and clock states, thus essentially behaving as mobile anchors, allowing a mobile transceiver to localize itself. The use of robots with multiple transceivers is proposed in [20] and [21], and in [22], a robot equipped with four transceivers localizes a mobile transceiver relative to itself by having one of the four transceivers actively range with the target and the other three passively listening.

In [23] and [24], a passive listening-based ranging protocol is proposed where the network is divided into "parent robots" that actively range with one another and "child robots" that passively listen in on these measurements. This hierarchical constraint has the limitation that parent robots cannot localize child robots and do not benefit from passive listening measurements themselves when they are not involved in a ranging transaction. In addition, it is suggested that the child robots use the estimated position and

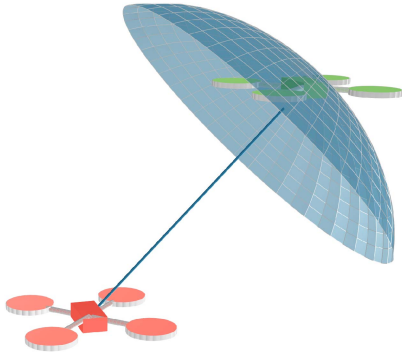


Fig. 3. Distribution of the posterior position of the green robot given a position prior and a single range measurement with the red robot.

clock states of the parent states, which in filtering applications would lead to untracked cross-correlations that would result in poor performance [25].

Furthermore, in filtering applications, the problem of communicating IMU measurements to neighbors remains unaddressed. In [26] and [27], scattering theory is used to send precomputed matrices between two robots rather than individual IMU measurements, in a manner similar to the concept of preintegration [1], [28]. However, extending this to more than two robots is challenging, particularly for preintegrated poses directly on $SE_2(3)$ [29], [30].

The motive behind using $SE_2(3)$ state representation for relative pose estimation using range measurements is due to this being inherently a nonlinear problem, which is commonly addressed using particle filtering [31], [32] to handle nonellipsoid-shaped distributions in Cartesian coordinates, see Fig. 3. This nonlinearity motivates the use of an on-manifold EKF, such as an EKF with states represented directly on the $SE_2(3)$ manifold, which can represent such nonellipsoid-shaped distributions using exponential coordinates [33].

III. PRELIMINARIES

A. Notation

Throughout this article, a bold upper-case letter (e.g., \mathbf{X}) denotes a matrix, a bold lower-case letter (e.g., \mathbf{x}) denotes a column matrix, and a right arrow under the letter (e.g., \underline{x}) denotes a physical vector. In a 3-D space, a vector \underline{x} resolved in a reference frame i is denoted as $\mathbf{x}_i \in \mathbb{R}^3$, while the derivative of a vector \underline{x} with respect to frame i is denoted as $\dot{\underline{x}}_i$.

The vector from point w to point z is denoted as \underline{r}_{zw} . The relative velocity and acceleration between points z and w with respect to frame i are denoted

$$\underline{v}_{zw/i} \triangleq \dot{\underline{r}}_{zw}, \quad \underline{a}_{zw/i} \triangleq \ddot{\underline{r}}_{zw/i}.$$

The rotation from a reference frame j to a reference frame i is parametrized using a rotation matrix $\mathbf{C}_{ij} \in SO(3)$. Therefore, the relationship between \mathbf{r}_i^{zw} and \mathbf{r}_j^{zw} is given by $\mathbf{r}_i^{zw} \equiv \mathbf{C}_{ij} \mathbf{r}_j^{zw}$.

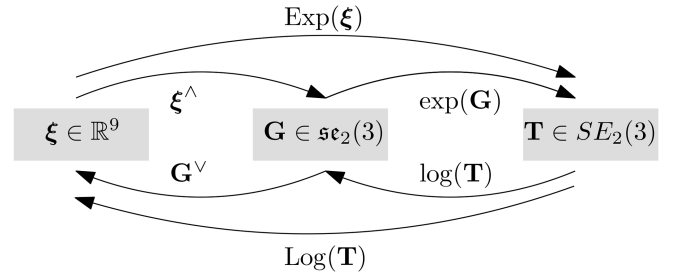


Fig. 4. Summary of the operators between elements of the different spaces associated with $SE_2(3)$.

Throughout this article, $\mathbf{1}$ and $\mathbf{0}$ denote identity and zero matrices of appropriate dimension, respectively. When ambiguous, a subscript will indicate the dimension of these matrices.

B. Matrix Lie Groups

The *pose* of one rigid body relative to another is defined using the relative attitude and position (\mathbf{C}, \mathbf{r}) , where all subscripts and superscripts are dropped in this section for conciseness. Meanwhile, the *extended pose* of one rigid body relative to another is defined using the relative attitude, velocity, and position $(\mathbf{C}, \mathbf{v}, \mathbf{r})$. The extended pose can be represented using an extended pose transformation matrix [29]

$$\mathbf{T} = \begin{bmatrix} \mathbf{C} & \mathbf{v} & \mathbf{r} \\ & \mathbf{1} & \\ & & 1 \end{bmatrix} \in SE_2(3),$$

where empty spaces represent $\mathbf{0}$ entries. The corresponding matrix Lie algebra is denoted as $\mathfrak{se}_2(3) \subset \mathbb{R}^{5 \times 5}$, and elements of this Lie algebra $\mathbf{G} \in \mathfrak{se}_2(3)$ can also be represented as elements of \mathbb{R}^9 by defining a linear mapping $(\cdot)^\wedge : \mathbb{R}^9 \rightarrow \mathfrak{se}_2(3)$ such that

$$\mathbf{G} = \xi^\wedge, \quad \xi \in \mathbb{R}^9.$$

Similarly, the inverse of $(\cdot)^\wedge$, denoted as $(\cdot)^\vee : \mathfrak{se}_2(3) \rightarrow \mathbb{R}^9$, is defined such that $\xi = \mathbf{G}^\vee$.

Mapping elements of the matrix Lie algebra $\mathfrak{se}_2(3)$ to the matrix Lie group $SE_2(3)$ is the *exponential map* $\exp : \mathfrak{se}_2(3) \rightarrow SE_2(3)$, thus yielding the definition

$$\mathbf{T} = \exp(\xi^\wedge) \triangleq \text{Exp}(\xi),$$

where $\text{Exp} : \mathbb{R}^9 \rightarrow SE_2(3)$ is defined for conciseness. The inverse of the exponential map is the *logarithmic map* $\log : SE_2(3) \rightarrow \mathfrak{se}_2(3)$, yielding the definition

$$\xi = \log(\mathbf{T})^\vee \triangleq \text{Log}(\mathbf{T}),$$

where $\text{Log} : SE_2(3) \rightarrow \mathbb{R}^9$ is defined for conciseness.

Because of the fact that $SE_2(3)$ is a matrix Lie group, the exponential map and logarithmic map are the same as the matrix exponential and the matrix logarithm, respectively. The operators between elements of the different spaces are summarized in Fig. 4, and their expression is found in [29], [30], and [34, Ch. 9]. Two other useful operators on $SE_2(3)$ are the *Adjoint matrix* $\text{Ad} : SE_2(3) \rightarrow \mathbb{R}^{9 \times 9}$ defined by

$$\text{Exp}(\text{Ad}(\mathbf{T})\xi) \triangleq \mathbf{T} \text{Exp}(\xi) \mathbf{T}^{-1},$$

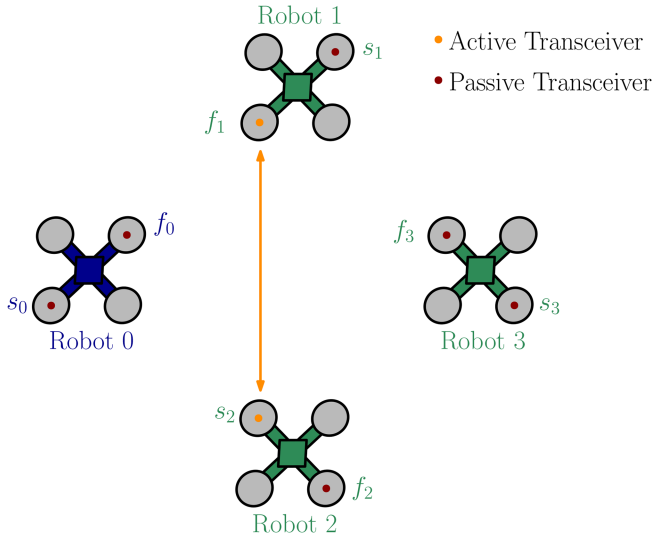


Fig. 5. Example of a ranging transaction, where Transceivers f_1 and s_2 are actively ranging with one another and all other tags are passively listening.

and the *odot* operator $(\cdot)^\odot : \mathbb{R}^5 \rightarrow \mathbb{R}^{5 \times 9}$ defined such that

$$\mathbf{p}^\odot \xi \triangleq \xi^\wedge \mathbf{p} \quad (1)$$

for any vector $\mathbf{p} \in \mathbb{R}^5$.

The noncommutativity of matrix multiplication means that matrix Lie group elements can be perturbed from the left $\mathbf{T} = \text{Exp}(\delta\xi)\bar{\mathbf{T}}$ or the right $\mathbf{T} = \bar{\mathbf{T}}\text{Exp}(\delta\xi)$, where the overbar denotes a nominal value. In addition, the first-order approximation

$$\text{Exp}(\delta\xi) \approx \mathbf{1} + \delta\xi^\wedge \quad (2)$$

will often be used when linearizing nonlinear models.

C. UWB Ranging and Clocks

UWB ranging between two transceivers relies on ToF measurements, which are deduced from timestamps recorded by a clock on each transceiver. However, these clocks are unsynchronized. Denoting $t_i(t)$ as the time t resolved in Transceiver i 's clock gives

$$t_i(t) = t + \tau_i(t), \quad (3)$$

where $\tau_i(t)$ defines the (time-varying) *offset* of clock i .

To obtain a range measurement, the two transceivers transmit and timestamp a sequence of messages among themselves, as shown between Robot 1 and Robot 2 in Fig. 6. A time instance corresponding to the i th message is denoted as T^i for the transmission time and R^i for the reception time, while a subscript j denotes the time instance as timestamped by Transceiver j . For example, $T_{f_0}^1$ is the timestamp corresponding to the first message transmission as recorded by Transceiver f_0 . The protocol example shown between Robot 1 and Robot 2 in Fig. 6 is a modified version of the standard double-sided two-way ranging (DS-TWR [35]) protocol as presented in [6], where the message shown in red represents an “information message” used to broadcast the timestamps recorded by Robot 1.

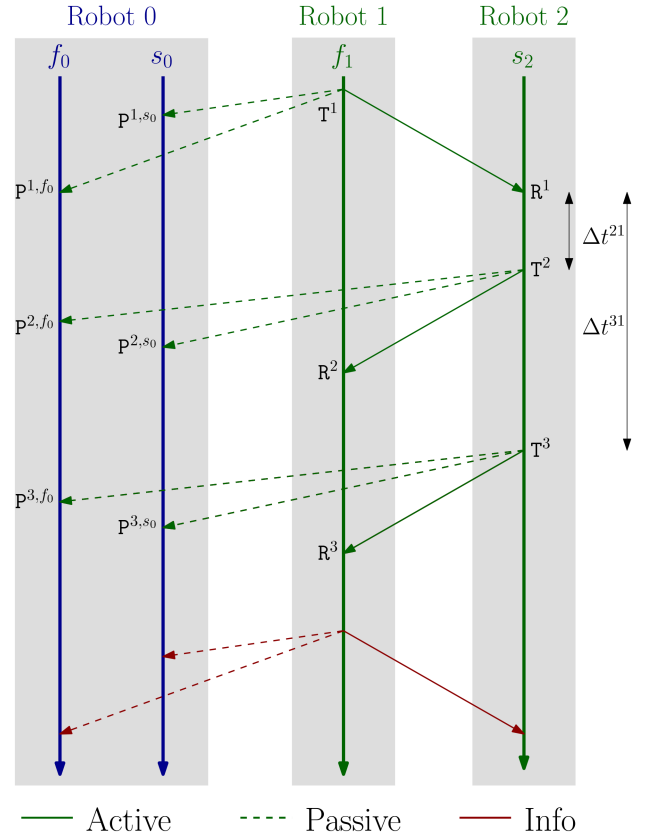


Fig. 6. Proposed ranging protocol when Transceiver f_1 is initiating a DS-TWR ranging transaction with Transceiver s_2 . This article proposes that all other transceivers listen in on these messages. Transceivers f_0 and s_0 on Robot 0 are passively listening, where the time instance corresponding to the i th passive reception at Transceiver j is denoted as $P^{i,j}$.

IV. PROBLEM FORMULATION

Consider a scenario with $n + 1$ robots, as shown in Fig. 5, for $n = 3$. Throughout this article, the perspective of one robot is considered, denoted without loss of generality Robot 0, as any of the $n + 1$ robots can be considered as Robot 0. Neighboring robots are then referred to as Robot i , where $i \in \{1, \dots, n\}$. This article employs a “robot-centric” viewpoint of the relative pose state estimation problem, where all states are estimated relative to Robot 0 and are resolved in the body frame of that robot. The robots are assumed to be rigid bodies, so any vector can be resolved in one of the following $n + 2$ reference frames:

- 1) an (absolute) inertial frame denoted with a subscript a ,
- 2) Robot 0's body frame denoted with a subscript 0, or
- 3) neighboring Robot i 's body frame denoted with a subscript i .

Each robot is equipped with an IMU at its center, consisting of a three-axis gyroscope and accelerometer. Given the use of accelerometers, the relative pose estimation problem involves estimating the extended pose of each neighboring robot relative to Robot 0 in Robot 0's body frame. The extended pose of Robot i is then defined as

$$\mathbf{T}_{0i} = \begin{bmatrix} \mathbf{C}_{0i} & \mathbf{v}_0^{i0/a} & \mathbf{r}_0^{i0} \\ & 1 & \\ & & 1 \end{bmatrix} \in SE_2(3), \quad i \in \{1, \dots, n\},$$

where time dependence is omitted from the notation for conciseness. The dependence on the absolute frame a is also omitted from the notation \mathbf{T}_{0i} , with the convention that all extended relative pose matrices in the article are of this form, where the vector corresponding to the second component in the first row is the derivative with respect to the *absolute* frame of the vector corresponding to the third component, irrespective of the fact that these vectors are resolved in frame 0.

Each robot is also equipped with two UWB transceivers for relative pose observability [20]. The *first* and *second* transceivers on Robot j are denoted f_j and s_j , respectively, for $j \in \{0, \dots, n\}$. It is assumed that the vector coordinates $\mathbf{r}_j^{f_j j}$ and $\mathbf{r}_j^{s_j j}$ between the transceivers and the IMU on Robot j are known, since they can be measured by hand or more accurately using a motion capture system.

Denote the set of all transceivers as $\mathcal{C} = \{f_0, \dots, f_n, s_0, \dots, s_n\}$. Consider the state of the clock on Transceiver $i \in \mathcal{C}$ relative to real time. The evolution of the offset $\tau_i(t)$ of clock i is modeled using a third-order model in [12]. However, [14] showed that a second-order model of the form

$$\underbrace{\begin{bmatrix} \dot{\tau}_i \\ \dot{\gamma}_i \end{bmatrix}}_{\mathbf{c}_i} = \underbrace{\begin{bmatrix} 0 & 1 \\ 0 & 0 \end{bmatrix}}_{\mathbf{A}} \underbrace{\begin{bmatrix} \tau_i \\ \gamma_i \end{bmatrix}}_{\mathbf{c}_i} + \mathbf{w}_i \quad (4)$$

is sufficient for localization purposes, where $\gamma_i(t)$ is called the *clock skew*, \mathbf{w}_i is a continuous-time zero-mean white Gaussian process noise with $\mathbb{E}[\mathbf{w}_i(t_1)\mathbf{w}_i(t_2)^\top] = \mathbf{Q}\delta(t_1 - t_2)$,

$$\mathbf{Q} = \begin{bmatrix} \mathcal{Q}^\tau & \\ & \mathcal{Q}^\gamma \end{bmatrix},$$

$\delta(\cdot)$ is the *Dirac's delta function*, and \mathcal{Q}^τ and \mathcal{Q}^γ are the clock offset and skew process-noise *power spectral densities*, respectively.

A robocentric viewpoint is also maintained for the clock states, where offsets and skews of all clocks are estimated relative to the clock of Transceiver f_0 on Robot 0. The clock state of Transceiver s_0 is then

$$\mathbf{c}_{s_0 f_0} = \begin{bmatrix} \tau_{s_0 f_0} \\ \gamma_{s_0 f_0} \end{bmatrix} \triangleq \begin{bmatrix} \tau_{s_0} - \tau_{f_0} \\ \gamma_{s_0} - \gamma_{f_0} \end{bmatrix} \in \mathbb{R}^2,$$

while the clock state of neighboring Robot i is given by

$$\mathbf{x}_{i0}^c \triangleq (\mathbf{c}_{f_i f_0}, \mathbf{c}_{s_i f_0}) \in \mathbb{R}^2 \times \mathbb{R}^2, \quad i \in \{1, \dots, n\},$$

where, as before, time dependence is omitted from the notation for conciseness. The full relative state estimate of Robot i is then given by

$$\mathbf{x}_{i0} \triangleq (\mathbf{T}_{0i}, \mathbf{x}_{i0}^c) \in SE_2(3) \times \mathbb{R}^2 \times \mathbb{R}^2,$$

and the full state estimated by Robot 0 is

$$\mathcal{X} \triangleq (\mathbf{c}_{s_0 f_0}, \mathbf{x}_{10}, \dots, \mathbf{x}_{n0}) \in \mathbb{R}^2 \times (SE_2(3) \times \mathbb{R}^2 \times \mathbb{R}^2)^n.$$

Communication constraints limit Robot 0's ability to estimate the state \mathcal{X} , since to prevent message collision only one pair of transceivers can communicate at a time. As the number of transceivers increases, this can result in poor scalability due to longer wait times between successive ranging measurements by a given pair. In addition, the rate at which transceivers communicate is typically lower than the rate at which IMU measurements are recorded at neighboring robots, thus Robot 0 cannot collect

the IMU measurements from all its neighbors without significant and impractical communication overhead. Therefore, part of the problem is to design a scalable and practical ranging protocol that accommodates these communication constraints.

This article presents an on-manifold EKF for estimating the state \mathcal{X} using a novel ranging protocol that allows all robots to listen in on neighbors while awaiting for their turn to communicate. It is known from [20] and [36] that the relative pose states are *observable* from IMU and range measurements. In particular, the use of two transceivers per robot ensures the observability of the relative poses while overcoming the need for *persistent excitation* or constant relative motion between the robots [20]. This benefit comes at the added cost of an additional transceiver. Nonetheless, UWB transceivers are typically compact, lightweight, low power, and inexpensive. In fact, the ones used in this article, as shown in Fig. 1, are 32 mm \times 49 mm in size and weigh approximately 8 g each. Meanwhile, assuming that the relative pose states are known since they are observable from the IMU and range measurements alone, clock offset measurements are sufficient to ensure observability of the clock states [14].

To simplify the analysis in this article, a complete communication graph with no packet drops or failures between the robots is assumed, which reduces the scalability of the system. Another factor impacting the scalability of the system is that the size of the state \mathcal{X} increases with n ; therefore, the number of robots that can be included in Robot 0's EKF is limited by Robot 0's computational capabilities. This article addresses scenarios where n is limited to a few robots. The complications associated with larger systems and incomplete and dynamic communication graphs are discussed in Section X-B.

V. RANGING PROTOCOL

A. Overview

To address the communication constraints, a ranging protocol is proposed that involves performing DS-TWR between all pairs of transceivers not on the same robot in sequence while leveraging passive listening measurements at all other transceivers that are not actively ranging. This is shown in Fig. 6 for an example where Transceiver f_1 is initiating a TWR transaction with Transceiver s_2 , and Transceivers f_0 and s_0 are passively listening. In the proposed ranging protocol, any of the $2(n+1)$ transceivers can initiate a TWR transaction with any of the $2n$ transceivers not on the same robot. In this section, the passive listening measurements are utilized in the relative pose state estimator as a source of ranging information between the different robots. This is possible due to the tightly-coupled nature of the proposed estimator, which performs both clock synchronization and relative pose estimation, meaning that clock-offset-corrupted passive listening measurements can still be used to correct relative pose states, as cross-correlation information is available between clock states and relative pose states at all times. There are multiple advantages to passive listening in multi-robot pose estimation applications, including the availability of more measurements for state correction, providing the robots with information-broadcasting ability, and allowing the implementation of simple MAC protocols.

Algorithm 1 The algorithm for the proposed ranging protocol when Transceiver f_1 is initiating the ranging transaction with Transceiver s_2 , and Transceivers f_0 , s_0 , s_1 , and f_2 are passively listening. Note that in this algorithm, the color blue is reserved for passive listening measurements that are available to the reference robot Robot 0, and the color teal is reserved for passive listening measurements at other robots that are not available to Robot 0.

Initiating Robot (Robot 1): The initiating robot has an active transceiver, f_1 , and a passive transceiver, s_1 .

- 1: Transmit message to s_2 , and timestamp T^1 in own clock.
- 2: Timestamp passive reception P^{1,s_1} in own clock, for message transmitted by f_1 .
- 3: Timestamp reception R^2 in own clock, for message transmitted by s_2 .
Timestamp passive reception P^{2,s_1} in own clock, for message transmitted by s_2 .
- 4: Timestamp reception R^3 in own clock and read R^1 , T^2 , T^3 , for message transmitted by s_2 .
Timestamp passive reception P^{3,s_1} in own clock, for message transmitted by s_2 .
- 5: Transmit info message with T^1 , R^2 , R^3 to s_2 .

Target Robot (Robot 2): The target robot has an active transceiver, s_2 , and a passive transceiver, f_2 .

- 1: Timestamp reception R^1 in own clock, for message transmitted by f_1 .
Timestamp passive reception P^{1,f_2} in own clock, for message transmitted by f_1 .
- 2: Transmit message to f_1 , and timestamp T^2 in own clock.
- 3: Timestamp passive reception P^{2,f_2} in own clock, for message transmitted by s_2 .
- 4: Set $T^3 = R^1 + \Delta t^{31}$, and wait until own clock is T^3 .
- 5: Transmit message with R^1 , T^2 , T^3 to f_1 .
- 6: Timestamp passive reception P^{3,f_2} in own clock, for message transmitted by s_2 .
- 7: Read T^1 , R^2 , R^3 from info message transmitted by f_1 .

Passive Robot (Robot 0): The passive robot has two passive transceivers, f_0 and s_0 .

- 1: Timestamp passive reception P^{1,f_0} in own clock, for message transmitted by f_1 .
Timestamp passive reception P^{1,s_0} in own clock, for message transmitted by f_1 .
 - 2: Timestamp passive reception P^{2,f_0} in own clock, for message transmitted by s_2 .
Timestamp passive reception P^{2,s_0} in own clock, for message transmitted by s_2 .
 - 3: Timestamp passive reception P^{3,f_0} in own clock and read R^1 , T^2 , T^3 , for message transmitted by s_2 .
Timestamp passive reception P^{3,s_0} in own clock, for message transmitted by s_2 .
 - 4: Read T^1 , R^2 , R^3 from info message transmitted by f_1 .
-

The rest of this section analyzes how the proposed ranging protocol can be used in a CSRPE. The particular scenario under study is the one, as shown in Figs. 5 and 6, where transceivers on two neighboring robots are the ones actively ranging. This is the most general case, and scenarios where one of the transceivers on Robot 0 is actively ranging involve similar but simpler derivations.

B. The Protocol

The ranging protocol proposed in this article involves two transceivers actively ranging with one another, while all other transceivers passively listen in on the messages. The actively ranging transceivers perform DS-TWR, as presented in [6]. The example shown in Fig. 6 is an example where Transceiver f_1 on Robot 1 initiates a transaction with Transceiver s_2 on Robot 2. Both robots have another transceiver, s_1 and f_2 for Robot 1 and Robot 2, respectively, which then passively listen to all the messages transmitted between the active transceivers. In addition, all other robots have both their transceivers passively listen to all the messages. For example, Robot 0 records passive listening measurements at both Transceivers f_0 and s_0 .

When the transceivers transmit and receive messages, whether actively or passively, the transceivers timestamp the time of transmission or reception. Each robot needs access to neighboring robots' timestamp measurements in order to be able to compute range measurements from the transaction. For example, Robot 0 needs access to the timestamps recorded by Transceivers f_1 and s_2 . As shown in Fig. 6, all timestamps are made available at Robot 0 at the end of the transaction by communicating all the timestamps recorded at Robot 1 in a final information message shown in red, and the timestamps recorded at Robot 2 are communicated in the last message transmitted by Robot 2. Note, however, that passive listening measurements recorded by the other transceivers on Robot 1, Robot 2, and any other neighboring robots are not made available to Robot 0. The ranging protocol is outlined in Algorithm 1 for the scenario shown in Fig. 6.

When implementing the ranging protocol, a choice has to be made on the receiving robot's side (in this case, Robot 2) for the delays $\Delta t^{21} \triangleq T^2 - R^1$ and $\Delta t^{31} \triangleq T^3 - R^1$. These user-defined parameters affect the frequency and noise of the measurements, and can be chosen based on [37]. Note that $\Delta t^{32} \triangleq \Delta t^{31} - \Delta t^{21}$. In addition, it will be assumed throughout this article that the distances between transceivers and the clock skews remain constant during one ranging transaction. These are good approximations for most robotic applications with typical clock rate variations [7, Ch. 7.1.4], [37].

The proposed ranging protocol has the following advantages. Given that all transceivers passively listen to neighboring robots communicating, this proposed protocol gives robots the ability to broadcast information, such as IMU measurements or estimated maps, at a higher rate as any robot can obtain information communicated between two neighboring robots. This feature will be utilized for multirobot preintegration in Section VII. In addition, given that each robot knows which robots are currently ranging, a simple MAC protocol can be implemented to prevent

message collision between multiple robots attempting to transmit messages at the same time. To do so, a user-defined sequence of ranging pairs can be made known to all robots. Each robot can then keep track of which pair in the sequence is currently ranging, and initiate a TWR transaction to a specified transceiver when it is its turn to do so. This MAC protocol is named here the *common-list protocol*.

C. Modeling Timestamp Measurements

The time instances shown in Fig. 6 are only available to the robots as noisy timestamps and in the clocks of the transceivers rather than in the global common time. Therefore, the timestamp measurements are affected by clock offsets, clock skews, and white noise. Modeling these effects, the timestamps available at Robot 1 (hereinafter, the *initiating robot*) are of the form

$$\tilde{T}_{f_1}^1 = T^1 + \tau_{f_1}(T^1) + \eta_{f_1}^1, \quad (5)$$

$$\tilde{R}_{f_1}^2 = T^1 + \frac{2}{c}d^{s_2f_1} + \Delta t^{21} + \tau_{f_1}(R^2) + \eta_{f_1}^2, \quad (6)$$

$$\tilde{R}_{f_1}^3 = T^1 + \frac{2}{c}d^{s_2f_1} + \Delta t^{31} + \tau_{f_1}(R^3) + \eta_{f_1}^3, \quad (7)$$

where $\tilde{(\cdot)}$ denotes a measured value, $d^{s_2f_1}$ is the distance between Transceivers s_2 and f_1 , and η_i^ℓ is the random noise on the ℓ th measurement of Transceiver i . All the random noise variables on timestamps are assumed to be independent, zero mean, and with the same variance σ^2 . Similarly, the measurements available at Robot 2 (hereinafter, the *target robot*) are of the form

$$\tilde{R}_{s_2}^1 = T^1 + \frac{1}{c}d^{s_2f_1} + \tau_{s_2}(R^1) + \eta_{s_2}^1, \quad (8)$$

$$\tilde{T}_{s_2}^2 = T^1 + \frac{1}{c}d^{s_2f_1} + \Delta t^{21} + \tau_{s_2}(T^2) + \eta_{s_2}^2, \quad (9)$$

$$\tilde{T}_{s_2}^3 = T^1 + \frac{1}{c}d^{s_2f_1} + \Delta t^{31} + \tau_{s_2}(T^3) + \eta_{s_2}^3. \quad (10)$$

The timestamp measurements (5)–(10) correspond to the standard DS-TWR protocol, from which ToF pseudomeasurements can be generated. Nonetheless, additional measurements are available at Robot 0 (hereinafter, the *passive robot*) since its transceivers f_0 and s_0 also receive the messages exchanged between the two actively ranging robots. This yields the following additional timestamp measurements at Robot 0

$$\tilde{P}_i^{1,i} = T^1 + \frac{1}{c}d^{f_1i} + \tau_i(P^{1,i}) + \eta_i^1, \quad (11)$$

$$\tilde{P}_i^{2,i} = T^1 + \frac{1}{c}d^{s_2f_1} + \frac{1}{c}d^{s_2i} + \Delta t^{21} + \tau_i(P^{2,i}) + \eta_i^2, \quad (12)$$

$$\tilde{P}_i^{3,i} = T^1 + \frac{1}{c}d^{s_2f_1} + \frac{1}{c}d^{s_2i} + \Delta t^{31} + \tau_i(P^{3,i}) + \eta_i^3, \quad (13)$$

where $i \in \{f_0, s_0\}$. Similarly, each neighboring robot not involved in the ranging transaction records its own passive listening measurements at its two transceivers. However, these are not shared with other robots as this would require each robot to take its turn transmitting a message.

In the case where Robot 0 is not involved in the ranging transaction and just listens in passively, there are 12 available timestamp measurements at Robot 0, six sent by neighboring robots, and three passive listening timestamps per transceiver

on Robot 0. However, when one of the transceivers f_0 or s_0 is involved in the ranging transaction, only nine timestamp measurements are available.

D. Pseudomeasurements as a Function of the State

To use the timestamp measurements (5)–(13) in the CSRPE, they must be rewritten as a function of the state being estimated. In this section, pseudomeasurements based on the timestamps available at Robot 0 after one TWR transaction are formulated to get models that are only a function of the states being estimated, as well as the known vectors between the transceivers and the IMUs resolved in the robot's body frame.

First, notice that the distance $d^{s_2f_1}$ between transceivers in (5)–(10) can be written as a function of the estimated states

$$\begin{aligned} d^{s_2f_1} &= \left\| \mathbf{r}_0^{s_2f_1} \right\| \\ &= \left\| \mathbf{r}_0^{s_20} - \mathbf{r}_0^{f_10} \right\| \\ &= \left\| (\mathbf{C}_{02}\mathbf{r}_2^{s_22} + \mathbf{r}_0^{20}) - (\mathbf{C}_{01}\mathbf{r}_1^{f_11} + \mathbf{r}_0^{10}) \right\| \\ &= \left\| \mathbf{\Pi} \left(\mathbf{T}_{02}\tilde{\mathbf{r}}_2^{s_22} - \mathbf{T}_{01}\tilde{\mathbf{r}}_1^{f_11} \right) \right\|, \end{aligned} \quad (14)$$

where $\|\cdot\|$ is the Euclidean norm, $\mathbf{\Pi} = [\mathbf{1}_3 \quad \mathbf{0}_{3 \times 2}] \in \mathbb{R}^{3 \times 5}$, and

$$\tilde{\mathbf{r}} = [\mathbf{r}^T \quad 0 \quad 1]^T.$$

To design the EKF, the linearization of (14) with respect to the state is shown in Appendix B.

Therefore, pseudomeasurements can be formed that are only a function of the distance between the transceivers, the clock states (relative to f_0), and the white timestamping noise. The **first pseudomeasurement** is the standard ToF measurement associated with DS-TWR [6], which from timestamps (5)–(10) can be written as

$$\begin{aligned} y^{\text{tof}} &= \frac{1}{2} \left(\left(\tilde{R}_{f_1}^2 - \tilde{T}_{f_1}^1 \right) - \frac{\tilde{R}_{f_1}^3 - \tilde{R}_{f_1}^2}{\tilde{T}_{s_2}^3 - \tilde{T}_{s_2}^2} \left(\tilde{T}_{s_2}^2 - \tilde{R}_{s_2}^1 \right) \right) \\ &\approx \frac{1}{c}d^{s_2f_1} + \frac{1}{2} \left(\eta_{f_1}^2 - \eta_{f_1}^1 - \eta_{s_2}^2 + \eta_{s_2}^1 \right). \end{aligned} \quad (15)$$

The relation (15) is obtained under the following approximations. First, clock skews γ_i are assumed constant over the duration of the transaction, where the transaction is in the order of a few milliseconds, so that during the transaction

$$\tau_i(t') - \tau_i(t) \approx \gamma_i(t' - t)$$

for any time instances t and t' and Transceiver i . Second, Δt^{21} , which like Δt^{32} is in the order of a few hundreds of microseconds, is much greater than $\frac{d}{c}$, and since clock skews are also small (in the order of a few parts-per-million [5]), then to first order $\gamma_i(R^2 - T^1) \approx \gamma_i\Delta t^{21}$. Third,

$$\frac{(1 + \gamma_{f_1})\Delta t^{32} + \eta_{f_1}^3 - \eta_{f_1}^2}{(1 + \gamma_{s_2})\Delta t^{32} + \eta_{s_2}^3 - \eta_{s_2}^2} \approx \frac{(1 + \gamma_{f_1})}{(1 + \gamma_{s_2})}$$

because the timestamping noise, in the order of a few hundred picoseconds at most, is much smaller than Δt^{32} . Finally,

$$\frac{(1 + \gamma_{f_1})}{(1 + \gamma_{s_2})} \left(\eta_{s_2}^2 - \eta_{s_2}^1 \right) \approx \eta_{s_2}^2 - \eta_{s_2}^1$$

to first order, because the clock skews and timestamping noise are both small.

The **second pseudomeasurement** is a direct clock offset measurement between the initiating and target transceivers, which from timestamps (5)–(10) can be written as

$$y^\tau = \frac{1}{2} \left((\tilde{\mathbf{R}}_{f_1}^2 + \tilde{\mathbf{T}}_{f_1}^1) - \frac{\tilde{\mathbf{R}}_{f_1}^3 - \tilde{\mathbf{R}}_{f_1}^2}{\tilde{\mathbf{T}}_{s_2}^3 - \tilde{\mathbf{T}}_{s_2}^2} (\tilde{\mathbf{T}}_{s_2}^2 - \tilde{\mathbf{R}}_{s_2}^1) - 2\tilde{\mathbf{R}}_{s_2}^1 \right) \\ \approx \tau_{f_1 f_0} - \tau_{s_2 f_0} + \frac{1}{2} (\eta_{f_1}^2 + \eta_{f_1}^1 - \eta_{s_2}^2 - \eta_{s_2}^1), \quad (16)$$

using the fact that $\tau_{f_1} - \tau_{s_2} = \tau_{f_1 f_0} - \tau_{s_2 f_0}$. Here and in the following, clock offsets are evaluated at time T^1 , which is omitted from the notation. This model is somewhat similar to the measurement model proposed in [14], but involves an additional term to correct the effect of the clock skew on the measured offset. In fact, the form of the first two pseudomeasurements is chosen to cancel out the terms $\frac{1}{2}(1 + \gamma_{f_1})\Delta t^{21}$ and $-\frac{1}{2}(1 + \gamma_{s_2})\Delta t^{21}$ by multiplying the latter with $\frac{1+\gamma_{f_1}}{1+\gamma_{s_2}}$.

The **third pseudomeasurement** is associated with the first passive listening timestamp, which is a function of the distance between the passive robot and the initiating robot, as well the clock offset between the two transceivers. Using timestamps (5) and (11) for $i \in \{f_0, s_0\}$, and $\tau_{f_0 f_0} \triangleq 0$, this is written as

$$y_i^{p,1} = \tilde{\mathbf{p}}_i^{1,i} - \tilde{\mathbf{T}}_{f_1}^1 = \frac{1}{c} d^{f_1 i} + \tau_{i f_0} - \tau_{f_1 f_0} + \eta_i^1 - \eta_{f_1}^1. \quad (17)$$

The **fourth pseudomeasurement** is similar to the third one, with an additional skew-correction component to model the passage of time Δt^{21} between the first and second signals in two clocks with different clock rates. Using timestamps (9) and (12) for $i \in \{f_0, s_0\}$, and $\gamma_{f_0 f_0} \triangleq 0$, this is modeled as

$$y_i^{p,2} = \tilde{\mathbf{p}}_i^{2,i} - \tilde{\mathbf{T}}_{s_2}^2 \\ = \frac{1}{c} d^{s_2 i} + \tau_{i f_0} - \tau_{s_2 f_0} \\ + (\gamma_{i f_0} - \gamma_{s_2 f_0})\Delta t^{21} + \eta_i^2 - \eta_{s_2}^2 \quad (18)$$

using the fact that $\gamma_i - \gamma_{s_2} = \gamma_{i f_0} - \gamma_{s_2 f_0}$. The exact delay Δt^{21} appearing in (18) is in fact unknown, as delay values are enforced by the transceivers in their own clocks. Nonetheless, to first order, the corresponding term can be replaced by

$$(\gamma_{i f_0} - \gamma_{s_2 f_0})\Delta t^{21} \approx (\gamma_{i f_0} - \gamma_{s_2 f_0})(\tilde{\mathbf{T}}_{s_2}^2 - \tilde{\mathbf{R}}_{s_2}^1).$$

Lastly, the **fifth pseudomeasurement** is similar to the fourth pseudomeasurement, but over a longer time window Δt^{31} . Using timestamps (10) and (13) for $i \in \{f_0, s_0\}$, this is modeled as

$$y_i^{p,3} = \tilde{\mathbf{p}}_i^{3,i} - \tilde{\mathbf{T}}_{s_2}^3 \\ = \frac{1}{c} d^{s_2 i} + \tau_{i f_0} - \tau_{s_2 f_0} \\ + (\gamma_{i f_0} - \gamma_{s_2 f_0})\Delta t^{31} + \eta_i^3 - \eta_{s_2}^3. \quad (19)$$

As before, Δt^{31} is unknown, but to first order

$$(\gamma_{i f_0} - \gamma_{s_2 f_0})\Delta t^{31} \approx (\gamma_{i f_0} - \gamma_{s_2 f_0})(\tilde{\mathbf{T}}_{s_2}^3 - \tilde{\mathbf{R}}_{s_2}^1).$$

Note the last three pseudomeasurements are per listening transceiver i , and therefore, there are a total of eight pseudomeasurements available at Robot 0 if it is not involved in the ranging transaction, or five pseudomeasurements if one

of the transceivers on Robot 0 is active. The additional pseudomeasurements available at the listening transceivers results in a $(1 + 3n)$ -fold increase in the total number of distinct measurements when considering a centralized approach where passive listening measurements from all robots are available, and a $(\frac{1}{2} + 2n)$ -fold increase in the number of distinct measurements when considering the perspective of an individual robot that does not have access to passive listening measurements at other robots. For example, for five neighboring robots, this results in a 16-fold and an 11.5-fold increase in the number of measurements, respectively. The former is purely due to passive listening measurements, while the latter is due to passive listening measurements as well as the ability to obtain direct ToF measurements between two neighboring robots. The proof of this claim is given in Appendix A.

E. Pseudomeasurements' Covariance Matrix

Given that the pseudomeasurements are a function of the same measured timestamps, cross-correlations between the pseudomeasurements exist and must be correctly modeled in the filter. Computing the variance of the pseudomeasurements (15)–(19) is straightforward, and can be summarized as

$$\mathbb{E}[(y^{\text{tof}} - \bar{y}^{\text{tof}})^2] = \sigma^2, \quad \mathbb{E}[(y^\tau - \bar{y}^\tau)^2] = \sigma^2,$$

$$\mathbb{E}[(y_i^{p,j} - \bar{y}_i^{p,j})^2] = 2\sigma^2, \quad j \in \{1, 2, 3\},$$

where an overbar denotes a noise-free value. Meanwhile, the cross-correlation between the ToF and offset measurements can be computed as $\mathbb{E}[(y^{\text{tof}} - \bar{y}^{\text{tof}})(y^\tau - \bar{y}^\tau)] = 0$ as the noise values are of alternating signs. Lastly, the cross-correlations between the passive listening measurements and the ToF measurements can be shown as follows

$$\mathbb{E}[(y_i^{p,1} - \bar{y}_i^{p,1})(y^{\text{tof}} - \bar{y}^{\text{tof}})] = \frac{1}{2}\sigma^2,$$

$$\mathbb{E}[(y_i^{p,2} - \bar{y}_i^{p,2})(y^{\text{tof}} - \bar{y}^{\text{tof}})] = \frac{1}{2}\sigma^2,$$

$$\mathbb{E}[(y_i^{p,3} - \bar{y}_i^{p,3})(y^{\text{tof}} - \bar{y}^{\text{tof}})] = 0,$$

while the cross-correlations with offset measurements are the same but with an opposite sign for the correlation with $y_i^{p,2}$. Passive listening measurements of different transceivers are also correlated. Stacking all the pseudomeasurements into one column matrix gives the random measurement vector

$$\mathbf{y} = \left[y^{\text{tof}} \quad y^\tau \quad y_{f_0}^{p,1} \quad y_{f_0}^{p,2} \quad y_{f_0}^{p,3} \quad y_{s_0}^{p,1} \quad y_{s_0}^{p,2} \quad y_{s_0}^{p,3} \right]^\top$$

with mean $\bar{\mathbf{y}}$ and covariance matrix \mathbf{R} , where

$$\mathbf{R} = \begin{bmatrix} \sigma^2 \mathbf{1}_2 & \frac{1}{2}\sigma^2 \mathbf{D} & \frac{1}{2}\sigma^2 \mathbf{D} \\ \frac{1}{2}\sigma^2 \mathbf{D}^\top & 2\sigma^2 \mathbf{1}_3 & \sigma^2 \mathbf{1}_3 \\ \frac{1}{2}\sigma^2 \mathbf{D}^\top & \sigma^2 \mathbf{1}_3 & 2\sigma^2 \mathbf{1}_3 \end{bmatrix}$$

and

$$\mathbf{D} = \begin{bmatrix} 1 & 1 & 0 \\ 1 & -1 & 0 \end{bmatrix}.$$

The measurement vector \mathbf{y} and its covariance \mathbf{R} are used in the correction step of an on-manifold EKF, where they are fused with the process model derived in the next section.

VI. PROCESS MODEL

To derive the process model, a Lie group referred to here as $DE_2(3)$ (D stands for *Delta*) with matrices of the form

$$\mathbf{U} = \begin{bmatrix} \mathbf{C} & \mathbf{v} & \mathbf{r} \\ & 1 & \Delta t \\ & & 1 \end{bmatrix} \in DE_2(3) \quad (20)$$

is introduced, where $\mathbf{C} \in SO(3)$, $\mathbf{v}, \mathbf{r} \in \mathbb{R}^3$, and $\Delta t \in \mathbb{R}$. The inverse of \mathbf{U} in (20) is

$$\mathbf{U}^{-1} = \begin{bmatrix} \mathbf{C}^T & -\mathbf{C}^T \mathbf{v} & -\mathbf{C}^T (\mathbf{r} - \Delta t \mathbf{v}) \\ & 1 & -\Delta t \\ & & 1 \end{bmatrix} \in DE_2(3).$$

Meanwhile, the adjoint operator satisfying

$$\text{Exp}(\text{Ad}(\mathbf{U})\boldsymbol{\xi}) \triangleq \mathbf{U} \text{Exp}(\boldsymbol{\xi}) \mathbf{U}^{-1}, \quad \text{Exp}(\boldsymbol{\xi}) \in SE_2(3)$$

is given by

$$\text{Ad}(\mathbf{U}) = \begin{bmatrix} \mathbf{C} & \mathbf{0} & \mathbf{0} \\ \mathbf{v}^\times \mathbf{C} & \mathbf{C} & \mathbf{0} \\ -(\Delta t \mathbf{v} - \mathbf{r})^\times \mathbf{C} & -\Delta t \mathbf{C} & \mathbf{C} \end{bmatrix},$$

where, for $\mathbf{v} = [v_1 \ v_2 \ v_3]^\top \in \mathbb{R}^3$,

$$\mathbf{v}^\times = \begin{bmatrix} 0 & -v_3 & v_2 \\ v_3 & 0 & -v_1 \\ -v_2 & v_1 & 0 \end{bmatrix}.$$

In addition, following the terminology in [34, Ch. 9], a *time machine* is a matrix \mathbf{M} of the form

$$\mathbf{M} = \begin{bmatrix} 1 & & & & \\ & 1 & \Delta t & & \\ & & & 1 & \\ & & & & 1 \end{bmatrix} \in \mathbb{R}^{5 \times 5},$$

where $\Delta t \in \mathbb{R}$. This allows writing \mathbf{U} in (20) as the product of two matrices

$$\mathbf{U} = \underbrace{\begin{bmatrix} 1 & & & & \\ & 1 & \Delta t & & \\ & & & 1 & \\ & & & & 1 \end{bmatrix}}_{\mathbf{M}} \underbrace{\begin{bmatrix} \mathbf{C} & \mathbf{v} & \mathbf{r} \\ & 1 & \\ & & 1 \end{bmatrix}}_{\mathbf{T} \in SE_2(3)}.$$

It can be shown that \mathbf{M} is in itself an element of a Lie group closed under matrix multiplication.

This section first extends the results in [34, Ch. 9] to address relative extended pose states. The clock-state process model is then derived. These are then used alongside the ranging protocol presented in Section V in the CSRPE.

A. Deriving the Extended Pose Process Model

The on-manifold relative pose kinematic model is first derived in continuous time as a function of the IMU measurements. The process model for the relative attitude between Robot 0 and Robot i is

$$\dot{\mathbf{C}}_{0i} = \mathbf{C}_{0i} (\boldsymbol{\omega}_i^{i0})^\times, \quad (21)$$

where $\boldsymbol{\omega}_i^{i0}$ is the angular velocity of Robot i 's body frame relative to Robot 0's body frame, resolved in Robot i 's body frame. However, the gyroscopes on Robots 0 and i measure $\boldsymbol{\omega}_0^{0a}$ and $\boldsymbol{\omega}_i^{ia}$, respectively. Therefore, (21) is rewritten as

$$\begin{aligned} \dot{\mathbf{C}}_{0i} &= \mathbf{C}_{0i} (\boldsymbol{\omega}_i^{ia} - \mathbf{C}_{0i}^T \boldsymbol{\omega}_0^{0a})^\times \\ &= -\mathbf{C}_{0i} (\mathbf{C}_{0i}^T \boldsymbol{\omega}_0^{0a})^\times + \mathbf{C}_{0i} (\boldsymbol{\omega}_i^{ia})^\times \end{aligned}$$

$$= -(\boldsymbol{\omega}_0^{0a})^\times \mathbf{C}_{0i} + \mathbf{C}_{0i} (\boldsymbol{\omega}_i^{ia})^\times. \quad (22)$$

Meanwhile, using the *transport theorem* [38, Ch. 2.10], the process model for the relative velocity of Robot i relative to Robot 0 is

$${}^0 \dot{\mathbf{v}}_i^{i0/a} = -\boldsymbol{\omega}_i^{0a} \times \mathbf{v}_i^{i0/a} + \underline{\boldsymbol{\alpha}}_i^{iw/a} - \underline{\boldsymbol{\alpha}}_i^{0w/a}, \quad (23)$$

where w is any point fixed to the reference frame a . Denoting the *specific forces* measured by the accelerometers as

$$\underline{\boldsymbol{\alpha}}_i^0 \triangleq \underline{\boldsymbol{\alpha}}_i^{0w/a} - \underline{\mathbf{g}}, \quad \underline{\boldsymbol{\alpha}}_i^i \triangleq \underline{\boldsymbol{\alpha}}_i^{iw/a} - \underline{\mathbf{g}},$$

where $\underline{\mathbf{g}}$ is the gravity vector, (23) can be written as

$${}^0 \dot{\mathbf{v}}_i^{i0/a} = -\boldsymbol{\omega}_i^{0a} \times \mathbf{v}_i^{i0/a} + \underline{\boldsymbol{\alpha}}_i^i - \underline{\boldsymbol{\alpha}}_i^0. \quad (24)$$

Similarly, the transport theorem gives the following process model for the position of Robot i relative to Robot 0

$${}^0 \dot{\mathbf{r}}_i^{i0} = -\boldsymbol{\omega}_i^{0a} \times \mathbf{r}_i^{i0} + \mathbf{v}_i^{i0/a}. \quad (25)$$

Lastly, resolving (24) and (25) in the body frame of Robot 0 and writing these equations as a function of the accelerometer-measured quantities $\boldsymbol{\alpha}_0^0$ and $\boldsymbol{\alpha}_i^i$ yields

$${}^0 \dot{\mathbf{v}}_0^{i0/a} = -(\boldsymbol{\omega}_0^{0a})^\times \mathbf{v}_0^{i0/a} + \mathbf{C}_{0i} \boldsymbol{\alpha}_i^i - \boldsymbol{\alpha}_0^0, \quad (26)$$

$${}^0 \dot{\mathbf{r}}_0^{i0} = -(\boldsymbol{\omega}_0^{0a})^\times \mathbf{r}_0^{i0} + \mathbf{v}_0^{i0/a}. \quad (27)$$

Combining (22), (26), and (27), the extended relative pose process model for Robot i can be written compactly as

$$\begin{aligned} \dot{\mathbf{T}}_{0i} &= \begin{bmatrix} \dot{\mathbf{C}}_{0i} & {}^0 \dot{\mathbf{v}}_0^{i0/a} & {}^0 \dot{\mathbf{r}}_0^{i0} \\ & 0 & 0 \\ & & 0 \end{bmatrix} \\ &= - \begin{bmatrix} (\boldsymbol{\omega}_0^{0a})^\times & \boldsymbol{\alpha}_0^0 & \\ & & 1 \\ & & 0 \end{bmatrix} \mathbf{T}_{0i} \\ &\quad + \mathbf{T}_{0i} \begin{bmatrix} (\boldsymbol{\omega}_i^{ia})^\times & \boldsymbol{\alpha}_i^i & \\ & & 1 \\ & & 0 \end{bmatrix} \\ &\triangleq -\tilde{\mathbf{U}}_0 \mathbf{T}_{0i} + \mathbf{T}_{0i} \tilde{\mathbf{U}}_i, \end{aligned} \quad (28)$$

with the matrices $\tilde{\mathbf{U}}_0$ and $\tilde{\mathbf{U}}_i$ containing the IMU measurements for Robot 0 and Robot i , respectively.

B. Discrete-Time Extended Pose Process Model

In order to discretize (28), the common assumption is made that accelerations and angular velocities are constant between IMU measurements, which is justified by the fact that IMU measurements typically occur at a high frequency (~ 100 – 1000 Hz). Consequently, since (28) is a *differential Sylvester equation*, and setting the initial condition to be $\mathbf{T}_{0i,k}$ at time-step k , a closed-form solution exists of the form [39]

$$\mathbf{T}_{0i,k+1} = \underbrace{\exp(\tilde{\mathbf{U}}_{0,k} \Delta t)^{-1}}_{\mathbf{U}_{0,k}^{-1}} \mathbf{T}_{0i,k} \underbrace{\exp(\tilde{\mathbf{U}}_{i,k} \Delta t)}_{\mathbf{U}_{i,k}}, \quad (29)$$

where Δt is the time interval between the IMU measurements at time-steps k and $k+1$.

Following a similar derivation as in [34, Ch. 9], expanding the matrix exponential is shown in Appendix C to yield a closed-form matrix of the form

$$\mathbf{U}_{0,k} = \begin{bmatrix} \text{Exp}(\boldsymbol{\Omega}_{0,k}) & \Delta t \mathbf{J}_l(\boldsymbol{\Omega}_{0,k}) \boldsymbol{\alpha}_{0,k}^0 & \frac{\Delta t^2}{2} \mathbf{N}(\boldsymbol{\Omega}_{0,k}) \boldsymbol{\alpha}_{0,k}^0 \\ 1 & & 1 \end{bmatrix},$$

where $\boldsymbol{\Omega}_{0,k} \triangleq \boldsymbol{\omega}_{0,k}^{0a} \Delta t$, and \mathbf{J}_l is the left Jacobian of $SO(3)$. Both \mathbf{J}_l and \mathbf{N} are defined in Appendix C. Note that $\mathbf{U}_{0,k}$ is an element of the aforementioned Lie group $DE_2(3)$. Similarly, $\mathbf{U}_{i,k} \in DE_2(3)$ is of the same form as $\mathbf{U}_{0,k}$ with the inputs being that of neighboring Robot i instead.

C. Linearizing the Extended Pose Process Model

To perform uncertainty propagation computations for the extended pose states, the process model is now linearized. Throughout this article, the state is perturbed on the left, as it yields simpler Jacobians. Nonetheless, a similar derivation can be done by perturbing the state on the right.

Perturbing (29) with respect to the state yields

$$\begin{aligned} \text{Exp}(\delta \boldsymbol{\xi}_{0i,k+1}) \bar{\mathbf{T}}_{0i,k+1} &= \bar{\mathbf{U}}_{0,k}^{-1} \text{Exp}(\delta \boldsymbol{\xi}_{0i,k}) \bar{\mathbf{T}}_{0i,k} \bar{\mathbf{U}}_{i,k} \\ &= \text{Exp}(\text{Ad}(\bar{\mathbf{U}}_{0,k}^{-1}) \delta \boldsymbol{\xi}_{0i,k}) \bar{\mathbf{U}}_{0,k}^{-1} \bar{\mathbf{T}}_{0i,k} \bar{\mathbf{U}}_{i,k}. \end{aligned}$$

Canceling out nominal terms and taking the $\text{Log}(\cdot)$ of both sides result in the linearized model

$$\delta \boldsymbol{\xi}_{0i,k+1} = \text{Ad}(\bar{\mathbf{U}}_{0,k}^{-1}) \delta \boldsymbol{\xi}_{0i,k}. \quad (30)$$

To perturb (29) with respect to the input noise, the aforementioned concept of time machines is used. The input matrix $\mathbf{U}_{0,k}$ can be written as

$$\begin{aligned} \mathbf{U}_{0,k} &= \mathbf{M} \begin{bmatrix} \text{Exp}(\boldsymbol{\Omega}_{0,k}) & \Delta t \mathbf{J}_l(\boldsymbol{\Omega}_{0,k}) \boldsymbol{\alpha}_{0,k}^0 & \frac{\Delta t^2}{2} \mathbf{N}(\boldsymbol{\Omega}_{0,k}) \boldsymbol{\alpha}_{0,k}^0 \\ 1 & & 1 \end{bmatrix} \\ &= \mathbf{M} \text{Exp} \left(\begin{bmatrix} \boldsymbol{\omega}_{0,k}^{0a} \Delta t \\ \boldsymbol{\alpha}_{0,k}^0 \Delta t \\ \frac{\Delta t^2}{2} \mathbf{J}_l(\boldsymbol{\Omega}_{0,k})^{-1} \mathbf{N}(\boldsymbol{\Omega}_{0,k}) \boldsymbol{\alpha}_{0,k}^0 \end{bmatrix} \right) \\ &= \mathbf{M} \text{Exp} \left(\underbrace{\begin{bmatrix} \Delta t \mathbf{1} & & \\ & \Delta t \mathbf{1} & \\ & & \frac{\Delta t^2}{2} \mathbf{J}_l(\boldsymbol{\Omega}_{0,k})^{-1} \mathbf{N}(\boldsymbol{\Omega}_{0,k}) \end{bmatrix}}_{\mathbf{V}_{0,k}} \underbrace{\begin{bmatrix} \boldsymbol{\omega}_{0,k}^{0a} \\ \boldsymbol{\alpha}_{0,k}^0 \end{bmatrix}}_{\mathbf{u}_{0,k}} \right) \\ &\triangleq \mathbf{M} \text{Exp}(\mathbf{V}_{0,k} \mathbf{u}_{0,k}) \end{aligned} \quad (31)$$

where $\mathbf{u}_{0,k} \in \mathbb{R}^6$ is Robot 0's IMU measurements or *input* at time-step k . Taking the perturbation of (31) with respect to the input yields

$$\begin{aligned} \mathbf{U}_{0,k} &\approx \mathbf{M} \text{Exp}(\bar{\mathbf{V}}_{0,k}(\bar{\mathbf{u}}_{0,k} + \delta \mathbf{u}_{0,k})) \\ &\approx \mathbf{M} \text{Exp}(\bar{\mathbf{V}}_{0,k} \bar{\mathbf{u}}_{0,k}) \text{Exp}(\mathcal{J}_l(-\bar{\mathbf{V}}_{0,k} \bar{\mathbf{u}}_{0,k}) \bar{\mathbf{V}}_{0,k} \delta \mathbf{u}_{0,k}) \\ &= \bar{\mathbf{U}}_{0,k} \text{Exp}(\mathcal{J}_l(-\bar{\mathbf{V}}_{0,k} \bar{\mathbf{u}}_{0,k}) \bar{\mathbf{V}}_{0,k} \delta \mathbf{u}_{0,k}) \\ &\triangleq \bar{\mathbf{U}}_{0,k} \text{Exp}(\mathbf{L}_{0,k} \delta \mathbf{u}_{0,k}), \end{aligned} \quad (32)$$

where input noise perturbations in $\mathbf{V}_{0,k}$ are neglected as the term $\frac{\Delta t^2}{2} \mathbf{J}_l(\boldsymbol{\Omega}_{0,k})^{-1} \mathbf{N}(\boldsymbol{\Omega}_{0,k})$ is small when the measurements are obtained using a high-rate IMU, $\mathbf{L}_{0,k} \triangleq \mathcal{J}_l(-\bar{\mathbf{V}}_{0,k} \bar{\mathbf{u}}_{0,k}) \bar{\mathbf{V}}_{0,k}$,

and $\mathcal{J}_l(\cdot)$ is the left Jacobian of $SE_2(3)$ [30, eq. (94)]. Similarly,

$$\mathbf{U}_{i,k} = \mathbf{M} \text{Exp}(\mathbf{V}_{i,k} \mathbf{u}_{i,k}) \approx \bar{\mathbf{U}}_{i,k} \text{Exp}(\mathbf{L}_{i,k} \delta \mathbf{u}_{i,k}). \quad (33)$$

Therefore, left-perturbing the state process model (29) with respect to the input noise yields

$$\begin{aligned} \text{Exp}(\delta \boldsymbol{\xi}_{0i,k+1}) \bar{\mathbf{T}}_{0i,k+1} &= \text{Exp}(-\mathbf{L}_{0,k} \delta \mathbf{u}_{0,k}) \bar{\mathbf{U}}_{0,k}^{-1} \bar{\mathbf{T}}_{0i,k} \bar{\mathbf{U}}_{i,k} \text{Exp}(\mathbf{L}_{i,k} \delta \mathbf{u}_{i,k}) \\ &= \text{Exp}(-\mathbf{L}_{0,k} \delta \mathbf{u}_{0,k}) \text{Exp}(\text{Ad}(\bar{\mathbf{T}}_{0i,k+1}) \mathbf{L}_{i,k} \delta \mathbf{u}_{i,k}) \bar{\mathbf{T}}_{0i,k+1}, \end{aligned}$$

which can then be simplified to give

$$\delta \boldsymbol{\xi}_{0i,k+1} = -\mathbf{L}_{0,k} \delta \mathbf{u}_{0,k} + \text{Ad}(\bar{\mathbf{T}}_{0i,k+1}) \mathbf{L}_{i,k} \delta \mathbf{u}_{i,k}. \quad (34)$$

It is worth mentioning that cross-correlations develop between relative pose states for all neighbors, because the noisy IMU measurements of Robot 0 are used to propagate all the relative pose states. These cross-correlations can be tracked using the models (30) and (34).

D. Discrete-Time Clock-State Process Model

The state dynamics for every clock is modeled as in (4). Nonetheless, the clock states relative to real time are unknown and unobservable. Therefore, clocks are modeled relative to clock f_0 , thus giving dynamics of the form

$$\dot{\mathbf{c}}_{if_0} = \mathbf{A} \mathbf{c}_{if_0} + \begin{bmatrix} -1 & 1 \end{bmatrix} \begin{bmatrix} \mathbf{w}_{f_0} \\ \mathbf{w}_i \end{bmatrix} \quad (35)$$

for $i \in \mathcal{C} \setminus \{f_0\}$. Discretizing (35) yields [40, Ch. 4.7]

$$\mathbf{c}_{if_0,k+1} = \mathbf{A}^d \mathbf{c}_{if_0,k} + \mathbf{w}_{if_0,k}, \quad (36)$$

where

$$\mathbf{A}^d = \exp(\mathbf{A} \Delta t) = \begin{bmatrix} 1 & \Delta t \\ & 1 \end{bmatrix},$$

$\mathbf{w}_{if_0,k} \sim \mathcal{N}(\mathbf{0}, \mathbf{Q}^d)$, and

$$\mathbf{Q}^d = 2 \begin{bmatrix} \Delta t \mathcal{Q}^\tau + \frac{1}{3} \Delta t^3 \mathcal{Q}^\gamma & \frac{1}{2} \Delta t^2 \mathcal{Q}^\gamma \\ \frac{1}{2} \Delta t^2 \mathcal{Q}^\gamma & \Delta t \mathcal{Q}^\gamma \end{bmatrix}.$$

Since the same noise \mathbf{w}_{f_0} appears in (35) for all $i \in \mathcal{C} \setminus \{f_0\}$, the process noise vectors $\mathbf{w}_{if_0,k}$ in (36) are jointly Gaussian but correlated, and one can show that their cross-covariance is

$$\mathbb{E}[\mathbf{w}_{if_0,k} \mathbf{w}_{jf_0,k}^\top] = \frac{1}{2} \mathbf{Q}^d,$$

for all $i, j \in \mathcal{C} \setminus \{f_0\}, i \neq j$.

VII. RELATIVE POSE STATE PREINTEGRATION

A. Need for Preintegration

When considering Robot 0's perspective, the estimated relative pose state is updated using (29) and the corresponding error covariance matrix using (30) and (34). Therefore, Robot 0 needs the IMU measurements of neighboring robots at every time-step in order to update its estimated state of its neighbors. This is limiting since robots cannot broadcast their IMU measurements at the same rate as they are recorded due to the possibility of message collision if multiple robots attempt to broadcast at the same time. In addition, to allow DS-TWR transactions to occur at the highest rate possible, the IMU information should ideally be transmitted using the ranging messages presented in Section V.

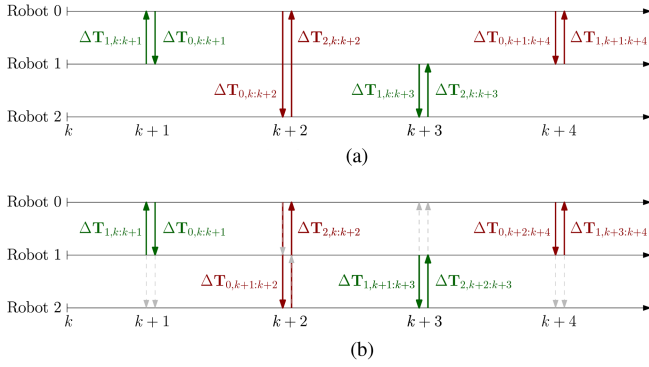


Fig. 7. Communicated RMIs with and without passive listening over a window of four ranging transactions, where $\Delta T_{i,\ell:m}$ is the RMI associated with the IMU measurements of Robot i from time-step ℓ to time-step $m-1$. (a) RMI communication without passive listening. (b) RMI communication with passive listening, where passive listening messages are shown using the gray arrows.

In this section, the concept of preintegration is proposed to compactly encode the IMU measurements of a neighboring Robot i over a window between two consecutive ranging instances using one *relative motion increment* (RMI), which is then sent over when Robot i ranges with one of its neighbors. However, as illustrated in Fig. 7(a), without passive listening the RMIs of Robot i become available to Robot 0 only when Robot 0 and Robot i communicate. Given that RMIs are computed iteratively as new IMU measurements arrive, each robot needs to keep track of one RMI per neighbor. For example, looking at Fig. 7(a) at time-step $k+3$, Robot 1 would be communicating the RMI of IMU measurements in the window k to $k+3$ to Robot 1, while also tracking a separate RMI for the window starting at $k+1$ to be sent to Robot 0 at time-step $k+4$.

On the other hand, passive listening over UWB lets two actively ranging robots broadcast their RMIs to all other robots, as shown in Fig. 7(b). This has the advantage that IMU information of neighbors becomes available faster at all robots, and the robots computing RMIs only need to track one RMI at all times since all neighbors are up-to-date with the most recently communicated RMI.

B. Relative Motion Increments

Consider the case where Robot i is an active robot only at nonadjacent time-steps ℓ and m . From (29), the relative pose state at time-step m can be computed from the relative pose state at time-step ℓ as

$$\mathbf{T}_{0i,m} = \left(\prod_{k=\ell}^{m-1} \mathbf{U}_{0,k} \right)^{-1} \mathbf{T}_{0i,\ell} \prod_{k=\ell}^{m-1} \mathbf{U}_{i,k}. \quad (37)$$

The inputs of Robot 0 are available at Robot 0 as soon as the measurements occur; therefore, the first term of (29) can be computed directly at every time-step. On the other hand, the inputs of Robot i from time-step ℓ to $m-1$ will only be available when the robot actively shares them at time-step m . Rather than sharing the individual IMU measurements, Robot i

can simply send

$$\Delta \mathbf{T}_{i,\ell:m} = \prod_{k=\ell}^{m-1} \mathbf{U}_{i,k} \in DE_2(3),$$

which is an RMI of the inputs of Robot i in the window ℓ to m . The process model representing time propagation between nonadjacent time-steps can then be rewritten as

$$\mathbf{T}_{0i,m} = \left(\prod_{k=\ell}^{m-1} \mathbf{U}_{0,k} \right)^{-1} \mathbf{T}_{0i,\ell} \Delta \mathbf{T}_{i,\ell:m}. \quad (38)$$

This is a feature of the process model (37) being reliant on the inputs of Robot i in a separable way, meaning that the inputs of Robot i can simply be post-multiplied in (37). Robot i computes its RMI iteratively, starting with $\Delta \mathbf{T}_{i,\ell,\ell} = \mathbf{1}$, and updating it when a new input measurement arrives as

$$\Delta \mathbf{T}_{i,\ell,k+1} = \Delta \mathbf{T}_{i,\ell,k} \mathbf{U}_{i,k}. \quad (39)$$

In order to linearize the RMI to be used in an EKF, a perturbation of the form

$$\Delta \mathbf{T}_{i,\ell,m} = \Delta \bar{\mathbf{T}}_{i,\ell,m} \text{Exp}(\delta \mathbf{w}_{i,\ell:m})$$

is defined, where $\delta \mathbf{w}_{i,\ell m} \in \mathbb{R}^9$ is some unknown noise parameter associated with the RMI, which is a consequence of the noise associated with every input measurement. Despite $\Delta \mathbf{T}_{i,\ell:m}$ being an element of $DE_2(3)$, the above Exp is the exponential operator in $SE_2(3)$. In addition, a right-perturbation is chosen to match the perturbation on \mathbf{U} derived in (33), which simplifies the subsequent derivation, but a left-perturbation could also have been chosen.

Perturbing (39) with respect to the RMI itself then yields

$$\begin{aligned} \Delta \bar{\mathbf{T}}_{i,\ell,k+1} \text{Exp}(\delta \mathbf{w}_{i,\ell,k+1}) &= \Delta \bar{\mathbf{T}}_{i,\ell,k} \text{Exp}(\delta \mathbf{w}_{i,\ell,k}) \bar{\mathbf{U}}_{i,k} \\ &= \Delta \bar{\mathbf{T}}_{i,\ell,k} \bar{\mathbf{U}}_{i,k} \text{Exp}(\text{Ad}(\bar{\mathbf{U}}_{i,k}^{-1}) \delta \mathbf{w}_{i,\ell,k}), \end{aligned}$$

which can be simplified to give

$$\delta \mathbf{w}_{i,\ell,k+1} = \text{Ad}(\bar{\mathbf{U}}_{i,k}^{-1}) \delta \mathbf{w}_{i,\ell,k}. \quad (40)$$

Meanwhile, perturbing the RMI relative to the input noise using (33) yields

$$\Delta \bar{\mathbf{T}}_{i,\ell,k+1} \text{Exp}(\delta \mathbf{w}_{i,\ell,k+1}) = \Delta \bar{\mathbf{T}}_{i,\ell,k} \bar{\mathbf{U}}_{i,k} \text{Exp}(\mathbf{L}_{i,k} \delta \mathbf{u}_{i,k}),$$

which can also be simplified to give

$$\delta \mathbf{w}_{i,\ell,k+1} = \mathbf{L}_{i,k} \delta \mathbf{u}_{i,k}. \quad (41)$$

C. Asynchronous-Input Filter

Taking advantage of the separability of the process model in the neighbor's input measurements, an asynchronous-input filter can be designed. The key idea here is to use two process models, one of the form

$$\mathcal{T}_{0i,k+1} = \mathbf{U}_{0,k}^{-1} \mathcal{T}_{0i,k}, \quad \mathcal{T}_{0i,k+1} \in DE_2(3) \quad (42)$$

at $\ell < k < m-1$ when there is no input information from Robot i , and another of the form

$$\mathbf{T}_{0i,m} = \mathbf{U}_{0,m-1}^{-1} \mathcal{T}_{0i,m-1} \Delta \mathbf{T}_{i,\ell:m} \quad (43)$$

when propagating from $k = m-1$ to m as Robot i communicates the RMI $\Delta \mathbf{T}_{i,\ell:m}$. Note that \mathcal{T} denotes an intermediate state estimate that is not an element of $SE_2(3)$. Only when the IMU measurements of the neighboring robot are incorporated does the estimated state restore its original $SE_2(3)$ form.

Algorithm 2: Algorithm for One Time-Step of the Proposed on-Manifold EKF Running on Robot 0.

The following is the pseudocode for Robot 0's EKF at time-step k . Let ℓ_p denote the last time Robot $p \in \{0, \dots, n\}$ communicated with one of its neighbors. Therefore, at time-step $k-1$, Robot 0 has the RMI $\Delta \mathbf{T}_{0,\ell_0:k-1}$, an intermediate estimate of neighboring robots' relative poses, $\hat{\mathbf{T}}_{0q,k-1}$, $q \in \{1, \dots, n\}$, as well as an estimate of the relative clock states. Robot 0 additionally gets an IMU measurement, allowing it to compute $\mathbf{U}_{0,k-1}$. The EKF is then as follows.

1: Propagate RMI using $\Delta \mathbf{T}_{0,\ell_0:k} = \Delta \mathbf{T}_{0,\ell_0:k-1} \mathbf{U}_{0,k-1}$ and its covariance using (40), (41).

2: **if** ranging with neighbor i **then**

3: Communicate $\Delta \mathbf{T}_{0,\ell_0:k}$ and its covariance.

4: Generate 5 pseudomeasurements using (15)–(19).

5: Propagate relative pose state estimates in time using

$$\check{\mathbf{T}}_{0p,k} = \mathbf{U}_{0,k-1}^{-1} \hat{\mathbf{T}}_{0p,k-1}, \quad p \in \{1, \dots, n\}, p \neq i,$$

$$\check{\mathbf{T}}_{0i,k} = \mathbf{U}_{0,k-1}^{-1} \hat{\mathbf{T}}_{0i,k-1} \Delta \mathbf{T}_{i,\ell_i:k},$$

and the clock state estimates using Section VI-D.

6: Propagate the state-error covariances using (44), (45) and Section VI-D.

7: Do an on-manifold EKF correction step [41] using the pseudomeasurements to get $\hat{\mathbf{T}}_{0p,k}$ and $\hat{\mathbf{T}}_{0i,k}$.

8: Initiate a new RMI $\Delta \mathbf{T}_{0,k:k} = \mathbf{1}$ with covariance $\mathbf{0}$.

9: **else if** neighbors i and j are ranging **then**

10: Generate 8 pseudomeasurements using (15)–(19).

11: Propagate relative pose state estimates in time using

$$\check{\mathbf{T}}_{0p,k} = \mathbf{U}_{0,k-1}^{-1} \hat{\mathbf{T}}_{0p,k-1}, \quad p \in \{1, \dots, n\}, p \neq i, j,$$

$$\check{\mathbf{T}}_{0i,k} = \mathbf{U}_{0,k-1}^{-1} \hat{\mathbf{T}}_{0i,k-1} \Delta \mathbf{T}_{i,\ell_i:k},$$

$$\check{\mathbf{T}}_{0j,k} = \mathbf{U}_{0,k-1}^{-1} \hat{\mathbf{T}}_{0j,k-1} \Delta \mathbf{T}_{j,\ell_j:k},$$

and the clock state estimates using Section VI-D.

12: Propagate the state-error covariances using (44), (45) and Section VI-D.

13: Do an on-manifold EKF correction step [41] using the pseudomeasurements to get $\hat{\mathbf{T}}_{0p,k}$, $\hat{\mathbf{T}}_{0i,k}$, and $\hat{\mathbf{T}}_{0j,k}$.

14: **else if** no one is ranging **then**

15: Propagate relative pose state estimates in time using

$$\check{\mathbf{T}}_{0p,k} = \mathbf{U}_{0,k-1}^{-1} \hat{\mathbf{T}}_{0p,k-1}, \quad p \in \{1, \dots, n\},$$

and the clock state estimates using Section VI-D.

16: Propagate the state-error covariances using (44) and Section VI-D.

17: **end if**

Given that (42) is of the same form as (29) with $\mathbf{U}_{i,k} = \mathbf{1}$, linearization is straightforward and follows Section VI-C

$$\delta \xi_{0i,k+1} = \text{Ad}(\bar{\mathbf{U}}_{0,k}^{-1}) \delta \xi_{0i,k} - \mathbf{L}_{0,k} \delta \mathbf{u}_{0,k}. \quad (44)$$

Similarly, (43) is of the same form as (29) with $\mathbf{U}_{i,k} = \Delta \mathbf{T}_{i,\ell_i:m}$, so the linearization with respect to the state is the same as (44), giving

$$\begin{aligned} \delta \xi_{0i,m} &= \text{Ad}(\bar{\mathbf{U}}_{0,m-1}^{-1}) \delta \xi_{0i,m-1} \\ &\quad - \mathbf{L}_{0,m-1} \delta \mathbf{u}_{0,m-1} + \text{Ad}(\bar{\mathbf{T}}_{0i,m}) \delta \mathbf{w}_{i,\ell_i:m}. \end{aligned} \quad (45)$$

A summary of the proposed on-manifold EKF is shown in Algorithm 2.

D. Equivalence to the No Communication Constraint Case

In the absence of communication constraints, each robot would have access to all its neighbors' IMU measurements at all times. As explained in Section VII-A, this is not possible, so that preintegration is needed. It is shown in (38) that the state can be propagated using RMIs in a manner equivalent to the case with no communication constraint. In this section, it is shown that computing the uncertainty propagation for the state is also equivalent in both cases, despite the Jacobians used being different. This is in fact a consequence of the structure of the Jacobians when perturbing the state from the left.

1) *No Communication Constraints:* When there are no communication constraints and IMU measurements of neighbors are available at all times, the models shown in Section VI can be used to propagate the state. The covariance of the state is propagated using (30) and (34), which for two nonadjacent timestamps ℓ and m would be written as

$$\begin{aligned} \delta \xi_{0i,m} &= \text{Ad}(\Delta \mathbf{T}_{0,\ell:m})^{-1} \delta \xi_{0i,\ell} - \sum_{k=\ell}^{m-1} \text{Ad}(\Delta \mathbf{T}_{0,k+1:m})^{-1} \mathbf{L}_{0,k} \delta \mathbf{u}_{0,k} \\ &\quad + \sum_{k=\ell}^{m-1} \text{Ad}(\Delta \mathbf{T}_{0,k+1:m}^{-1} \bar{\mathbf{T}}_{0i,k+1}) \mathbf{L}_{i,k} \delta \mathbf{u}_{i,k}. \end{aligned} \quad (46)$$

2) *With Preintegration:* First, the uncertainty of the RMI can be computed using (40) and (41) as

$$\delta \mathbf{w}_{i,\ell:m} = \sum_{k=\ell}^{m-1} \text{Ad}(\Delta \mathbf{T}_{i,k+1:m})^{-1} \mathbf{L}_{i,k} \delta \mathbf{u}_{i,k}.$$

Note that the RMI gets communicated at time-step m , so from time-step ℓ to $m-1$ the state propagation occurs only with the IMU measurements of Robot 0 as shown in (42). The uncertainty propagation from timestamp ℓ to $m-1$, then, follows as per (44), which can be written as

$$\begin{aligned} \delta \xi_{0i,m-1} &= \text{Ad}(\Delta \mathbf{T}_{0,\ell:m-1})^{-1} \delta \xi_{0i,\ell} \\ &\quad - \sum_{k=\ell}^{m-2} \text{Ad}(\Delta \mathbf{T}_{0,k+1:m-1})^{-1} \mathbf{L}_{0,k} \delta \mathbf{u}_{0,k}. \end{aligned}$$

Meanwhile, propagating the uncertainty from timestamp $m-1$ to m using the RMI as shown in (43), then, follows as per (45) to give

$$\begin{aligned} \delta \xi_{0i,m} &= \text{Ad}(\Delta \mathbf{T}_{0,\ell:m})^{-1} \delta \xi_{0i,\ell} - \sum_{k=\ell}^{m-1} \text{Ad}(\Delta \mathbf{T}_{0,k+1:m})^{-1} \mathbf{L}_{0,k} \delta \mathbf{u}_{0,k} \\ &\quad + \text{Ad}(\Delta \mathbf{T}_{0,\ell:m}^{-1} \bar{\mathbf{T}}_{0i,\ell} \Delta \mathbf{T}_{i,\ell:m}) \delta \mathbf{w}_{i,\ell:m} \\ &= \text{Ad}(\Delta \mathbf{T}_{0,\ell:m})^{-1} \delta \xi_{0i,\ell} - \sum_{k=\ell}^{m-1} \text{Ad}(\Delta \mathbf{T}_{0,k+1:m})^{-1} \mathbf{L}_{0,k} \delta \mathbf{u}_{0,k} \\ &\quad + \sum_{k=\ell}^{m-1} \text{Ad}(\Delta \mathbf{T}_{0,k+1:m}^{-1} \Delta \mathbf{T}_{0,\ell:k+1}^{-1} \bar{\mathbf{T}}_{0i,\ell} \Delta \mathbf{T}_{i,\ell:k+1}) \mathbf{L}_{i,k} \delta \mathbf{u}_{i,k}, \end{aligned}$$

which, using (38), simplifies to be exactly equal to (46).

E. Communication Requirements

The proposed multi-robot preintegration approach provides an alternative efficient way of communicating odometry information as compared with communicating the individual IMU measurements. When sending IMU measurements, no covariance information is required as the covariance matrix is typically a fixed value that can be assumed common among all robots if they all share the same kind of IMU. Meanwhile, when sending an RMI, the components of a corresponding 9×9 positive-definite symmetric matrix representing its computed uncertainty must also be sent, as this is not constant but rather a function of the individual inputs.

Each IMU measurement consists of six single-precision floats, three for the gyroscope, and three for the accelerometer readings, for a total of 24 bytes. Meanwhile, each RMI can be represented using ten single-precision floats and the corresponding covariance matrix using the upper triangular part of the 9×9 matrix, which requires communicating additional 45 single-precision floats. Therefore, sending one RMI and its covariance matrix requires over 220 bytes of information. As such, unless an RMI replaces more than nine IMU measurements, it is sometimes more efficient to communicate the raw IMU measurements. Nonetheless, using the proposed multirobot preintegration framework has the following advantages (in addition to the discussion in Section VII-A).

- 1) It overcomes the need for variable amount of communication, as the RMI and its covariance matrix are of fixed length but a varying number of IMU readings might be accumulated in between two instances of a robot ranging. This consequently eases implementation and provides a more reliable system.
- 2) It provides robustness to loss of communication, as a robot re-establishing communication with its neighbors after a few seconds would not be able to send over all the accumulated IMU information.
- 3) It reduces the amount of processing required at neighbors, as the input matrices $\mathbf{U}_{i,k}$ are premultiplied at Robot i on behalf of all its neighbors.
- 4) It overcomes the need to know the noise distribution of the neighbors' IMUs, which would be useful if not all robots had the same IMU.
- 5) It allows easy integration with IMU-bias estimators and approaches that dynamically tune the covariance of the IMU measurements, without needing to send the bias estimates or the tuned covariances over UWB.

In addition, UWB protocols by default allow 128 bytes of information to be sent per message transmission [42], for a total of 256 bytes per transceiver in each TWR instance. Given that each transceiver only needs to send 2 bytes of frame-control data per signal (thus, 4 bytes of frame-control data in total) [42] and a total of three single-precision timestamps (thus, 12 bytes of timestamps), there is enough room for 220 bytes required to send an RMI. Note that if more information is required, some modules, such as DW1000, allow up to 1024 bytes of data per message transmission [43].

TABLE I
SIMULATION PARAMETERS BASED ON THE ICM-20689 IMU AND THE
DWM1000 UWB TRANSCEIVER

Specification	Value
Accelerometer std. dev. [m/s ²]	0.023
Gyroscope std. dev. [rad/s]	0.0066
IMU rate [Hz]	250
UWB timestamping std. dev. [ns]	0.33
UWB rate [Hz]	125
Clock offset PSD [ns ² /Hz]	0.4
Clock skew PSD [ppb ² /Hz]	640

VIII. SIMULATION RESULTS

To evaluate the benefits of using passive listening on the estimation accuracy of relative pose states, the clock dynamics and quadcopter kinematics have been simulated. The clocks' evolution is modeled relative to a "global time" using the simulating computer's own clock, while the absolute-state quadcopter kinematics are simulated relative to some inertial frame. Noisy IMU and timestamp measurements are then modeled and fed into the CSRPE algorithm to estimate the relative clock and pose states.

To evaluate the proposed approach, the following three datasets are simulated.

- 1) *S1*: A single run with four quadcopters.
- 2) *S2*: In total, 100 Monte Carlo trials with 3–7 quadcopters.
- 3) *S3*: In total, 500 Monte Carlo trials with four quadcopters.

The trajectory of the quadcopters in the case of a system with three robots is shown in Fig. 2, and the simulation parameters are given in Table I. The simulated trajectories are 60 s long, and each quadcopter covers a distance between 60 and 218 m, with a maximum speed of 5.5 m/s. The maximum and mean angular velocities are 1 and 0.3 rad/s, respectively. Following a periodic sequence, each pair of transceivers performs in turn a ranging transaction, except for pairs of transceivers on the same robot. The proposed algorithm is then tested on each dataset and compared with the following two scenarios.

- 1) *Centralized*: A hypothetical centralized scenario where each robot has access to range measurements between neighbors in the absence of passive listening. This differs from the proposed framework in that the pseudomeasurements associated with passive listening do not exist, and that this is practically impossible without passive listening or some other communication media. This serves as the benchmark on what is the best achievable estimator using existing methods.
- 2) *No Passive Listening*: A decentralized approach but in the absence of passive listening, meaning that robots neither have access to the passive listening pseudomeasurements nor range measurements between neighbors. This serves as the benchmark on what is currently a practically implementable solution without requiring a central processor or additional communication media.

The evaluation is based on the following three criteria.

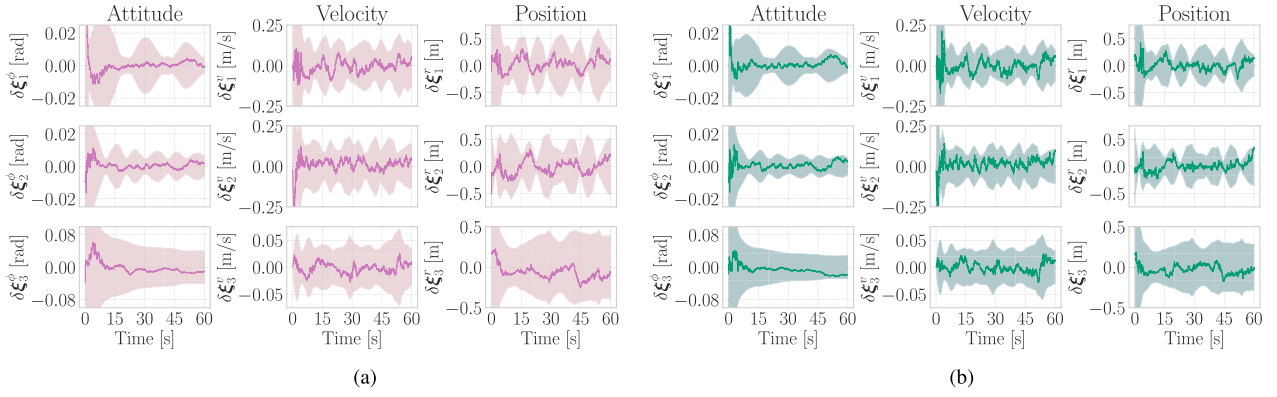


Fig. 8. Error plots and $\pm 3\sigma$ bounds (shaded region) for Robot 0's estimate of Robot 1's relative pose for Simulation S1, comparing the centralized and proposed approaches. (a) Centralized. (b) With passive listening.

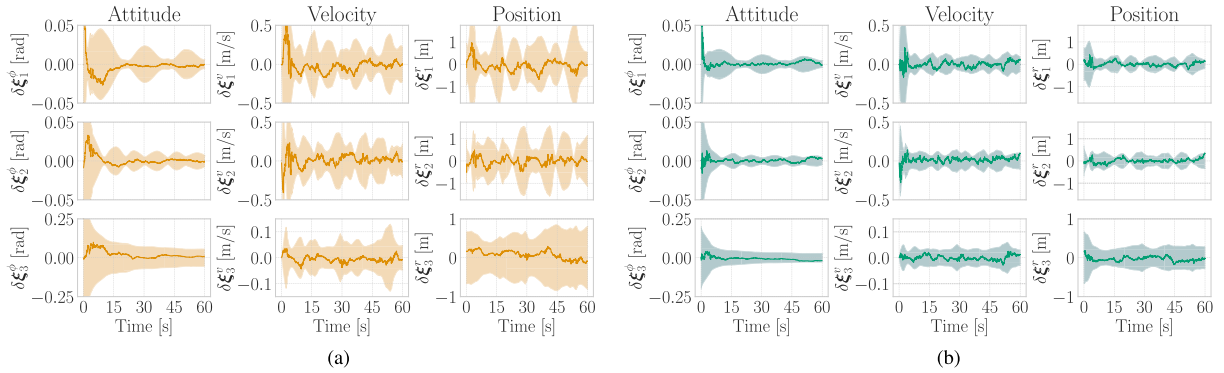


Fig. 9. Error plots and $\pm 3\sigma$ bounds (shaded region) for Robot 0's estimate of Robot 1's relative pose for Simulation S1, comparing the decentralized no-passive listening and proposed approaches. The right figure is a zoomed-out version of Fig. 8(b). (a) No passive listening. (b) With passive listening.

- 1) *Accuracy*: The accuracy of the proposed algorithm as compared with the case with no passive listening is quantified using error plots and the *root-mean-squared-error* (RMSE), which for the pose estimation error $\mathbf{e}_k = \text{Log}(\hat{\mathbf{T}}_k \mathbf{T}_k^{-1})$ is computed as

$$\text{RMSE} \triangleq \sqrt{\frac{1}{N+1} \sum_{k=0}^N \mathbf{e}_k^T \mathbf{e}_k}$$

for $N+1$ time-steps.

- 2) *Precision*: The precision of the proposed algorithm is quantified using $\pm 3\sigma$ -bound regions about the estimate, which represent a 99.73% confidence bound under a Gaussian distribution assumption.
- 3) *Consistency*: A consistent estimator is an estimator with a modeled precision that reflects the true precision of its estimate. In more specific terms, a consistent estimator outputs a covariance matrix on its estimate that is representative of the true uncertainty of that estimate. Consistency is evaluated using the *normalized-estimation-error-squared* (NEES) test [44, Sec. 5.4].

A. Estimation Accuracy and Precision

The error plots for the relative pose estimate of Robot 1 relative to Robot 0 in Simulation S1 are shown in Figs. 8 and 9. Passive listening reduces the positioning RMSE by 29.4% from 0.204 to 0.144 m as compared with the centralized approach,

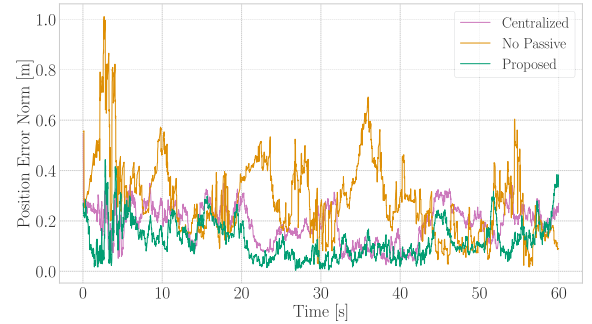


Fig. 10. Error norm for Robot 0's estimate of Robot 1's relative pose for Simulation S1.

and by 55.96% from 0.327 to 0.144 m when compared with the case of no passive listening. In addition, passive listening produces at almost every time-step a position error with smaller norm, as shown in Fig. 10. The proposed estimator is also significantly more confident in its estimate, as shown by the covariance bounds in Figs. 8 and 9.

This improvement in localization performance can be attributed to more measurements and stronger cross-correlation between the different states when passive listening measurements are available. As shown in Fig. 11, passive listening results in the clock state of a transceiver not drifting significantly in between instances where this transceiver is ranging. This brings

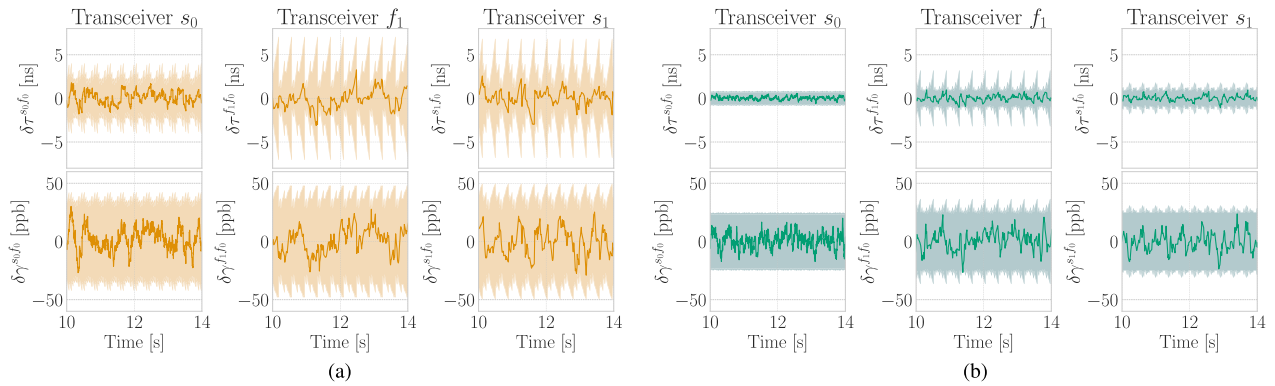


Fig. 11. Error plots and $\pm 3\sigma$ bounds (shaded region) for Robot 0's estimate of the clock states of Transceivers s_0 , f_1 , and s_1 relative to Transceiver f_0 for Simulation S1. These plots are zoomed in to a window of 4 s to show clearly the cycle of expanding and contracting uncertainty in the clock estimates as the transceiver alternates between active ranging and passive listening. (a) No passive listening. (b) With passive listening.

TABLE II
AVERAGE RMSE (ARMSE) FOR ALL TRIALS OF ROBOT 0'S ESTIMATE OF NEIGHBORING ROBOTS' RELATIVE POSE FOR SIMULATION S2

Number of Robots	Position aRMSE averaged over all Robots [m]			Percentage change [%]	
	Centr.	No Passive	Proposed	Centr.	No Passive
3	0.277	0.486	0.263	-5.05	-45.88
4	0.231	0.574	0.222	-3.90	-61.32
5	0.220	0.662	0.211	-4.09	-68.13
6	0.220	0.737	0.199	-9.55	-73.00
7	0.186	0.917	0.165	-11.29	-82.01

down the clock offset RMSE of Transceiver f_1 , for example, by 59.31% from 1.155 to 0.470 ns when compared with the case with no passive listening.

The improvement in performance can also be seen as the number of robots is increased, as given in Table II for the Simulation S2. Because only one pair of transceivers can communicate at a time, in the absence of passive listening the rate at which each transceiver participates in a ranging transaction decreases with the number of transceivers, and as a result the overall localization performance degrades. With passive listening on the other hand, adding robots does not result in longer periods without measurements and the measurement rate per robot remains the same. In fact, it turns out that adding robots in the presence of passive listening produces better performance due to spatial variations in the range-measurement sources [45]. This is also the case for the centralized estimator.

To provide further insight into the contribution of passive listening measurements on the behavior of the estimator, the distribution of the RMSEs of the position and attitude estimates of all robots in Simulation S3 are visualized in Fig. 12. Not only does the proposed approach significantly outperform the no passive listening approach, but it also matches the centralized approach, which is typically the best possible solution under an assumption of the availability of a central processor. In fact, the proposed framework slightly outperforms the standard

centralized approach due to the availability of additional pseudomeasurements.

B. Consistency

Given that the estimator is an EKF, consistency cannot be guaranteed due to linearization and discretization errors. Nonetheless, the proposed on-manifold framework can characterize banana-shaped error distributions that result from range measurements, as shown in Fig. 3 more efficiently. Consequently, the error distribution appears to be well characterized by the estimator, as shown in Figs. 8–11, as the error trajectory typically lies within the $\pm 3\sigma$ bounds.

A better evaluation of the consistency of the estimator is a NEES test, which is performed over the 500 trials of Simulation S3, and is shown in Fig. 13. During the first few seconds when the quadcopters are taking OFF from the ground, their geometry and low speeds result in a weakly observable system [36], which results in overconfidence of the estimator as linearization-based filters can correct in unobservable directions [46], [47]. Nonetheless, the estimator then converges toward consistency, although it is never perfectly consistent due to linearization and discretization errors, which is a feature of EKFs. This can be solved by slightly inflating the associated covariance matrices used in the filter.

IX. EXPERIMENTAL RESULTS

The proposed approach is tested on multiple experimental trials. The ranging protocol discussed in Section V is implemented in C on custom-made boards fitted with DWM1000 UWB transceivers [43]. Two boards are then fitted to Uvify IFO-S quadcopters approximately 45 cm apart. The experimental setup is shown in Fig. 1. Three of these quadcopters are then used for the experimental results shown in this section, with multiple trajectories approximately 75 s long similar to the one shown in Fig. 14 in a roughly 5 m \times 5 m area. The quadcopters in the experimental trajectories each cover a distance between 20 and 35 m, with a maximum speed of 3.75 m/s. The maximum and mean angular velocities are 2.12 and 0.3 rad/s, respectively. In order to analyze the error in the pose estimates of the robots, a

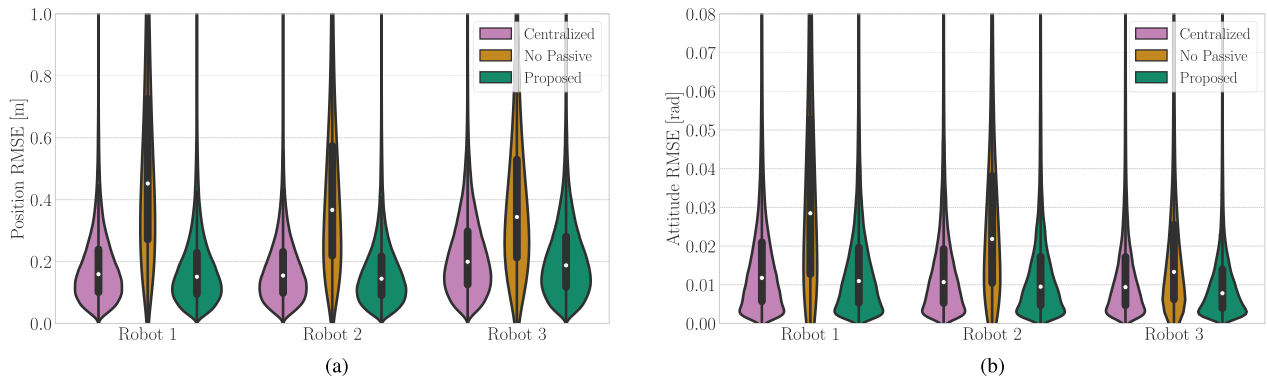


Fig. 12. Violin and box plots showing the distribution of the position and attitude RMSEs for Simulation S3. The envelope shows the relative frequency of RMSE values. The box plot shows the median as a white dot, while the first and third quartile of the data are represented using the lower and upper bound of the thick black bar, respectively. (a) Position RMSE. (b) Attitude RMSE.

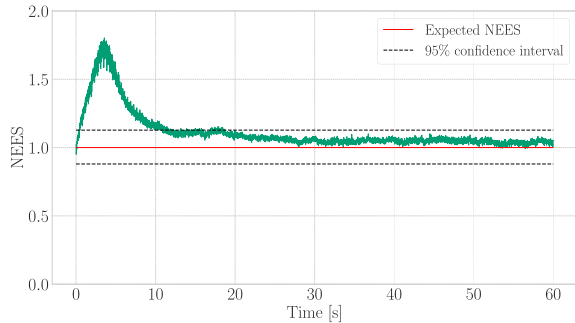


Fig. 13. 500-trial NEES plot for the proposed estimator on Simulation S3.

12-camera Vicon motion-capture system is used to record the ground-truth pose of each quadcopter.

To enable the six transceivers to take turn ranging, the common-list protocol discussed in Section V is implemented using the *robot operating system* (ROS). This allows each robot to range with its neighbors at a rate of 90 Hz, and collect passive listening measurements at a rate of 150 Hz. These UWB measurements are corrected for antenna delays and power-induced biases using [6], before fusing them with the onboard IMU and height measurements in the proposed EKF. An ICM-20689 IMU is used with characteristics similar to the simulated ones given in Table I, and the height measurements are obtained from a downward-facing camera. The height measurement error is assumed Gaussian with 5 cm of standard deviation. To reject outliers in the range and passive listening measurements, the *normalized-innovation-squared* test is used in the filter [44, Sec. 5.4].

Note that before flight, all transceivers are allowed to range with one another to initialize the relative clock offset states using the second pseudomeasurement from Section V, alongside a pseudomeasurement $y^\gamma = \frac{\hat{\mathbf{R}}^3 - \hat{\mathbf{R}}^2}{\hat{\mathbf{T}}^3 - \hat{\mathbf{T}}^2} - 1 \approx \gamma_{f_1} s_2$ that is not used in the filter. Meanwhile, the IMU biases are initialized using the motion capture system and are then assumed constant throughout the experiment, which is sufficient for the duration of the experiments presented here. Addressing IMU biases for longer experiments is presented in Section X-A.

TABLE III
RMSE OF ROBOT 0'S ESTIMATE OF NEIGHBORING ROBOTS' RELATIVE POSE FOR MULTIPLE EXPERIMENTAL TRIALS

	Position RMSE averaged over all Robots [m]			Percentage change [%]	
	Centr.	No Passive	Proposed	Centr.	No Passive
Trial 1	0.390	0.437	0.341	-12.56	-21.97
Trial 2	0.614	0.954	0.576	-6.19	-39.62
Trial 3	0.462	0.593	0.443	-4.11	-25.30
Trial 4	0.580	0.859	0.445	-23.28	-48.20

The pose-error plots for one of the trials are shown in Fig. 15 for the centralized approach, and with and without fusing passive listening measurements. The RMSE comparison for four different trials with varying motion are given in Table III. Although all scenarios result in error trajectories that fall within the error bounds, it is clear that with the additional passive listening measurements available to the robot at 150 Hz, the relative position estimates in particular become significantly less uncertain. In addition, these error plots correspond to the first row in Table III, showing that the improvement in the confidence of the estimator is additionally accompanied with a 12.56% and 21.97% reduction in the RMSE as compared with the centralized and no passive listening position RMSE, respectively. This reduction in RMSE goes up to 23.28% and 48.20%, respectively, for one of the runs when passive listening measurements are utilized.

X. FURTHER PRACTICAL CONSIDERATIONS

A. IMU Biases

The IMU measurements typically suffer from time-varying biases, which must be estimated as part of the state for long-term navigation. It can be shown that, when modeling the evolution of biases as a random walk, the IMU biases can be incorporated into the process model while still maintaining the differential Sylvester equation form presented in Section VI-A. To do so, each Robot i estimates its own gyroscope bias $\beta_i^{\text{gyr},i}$ in its own

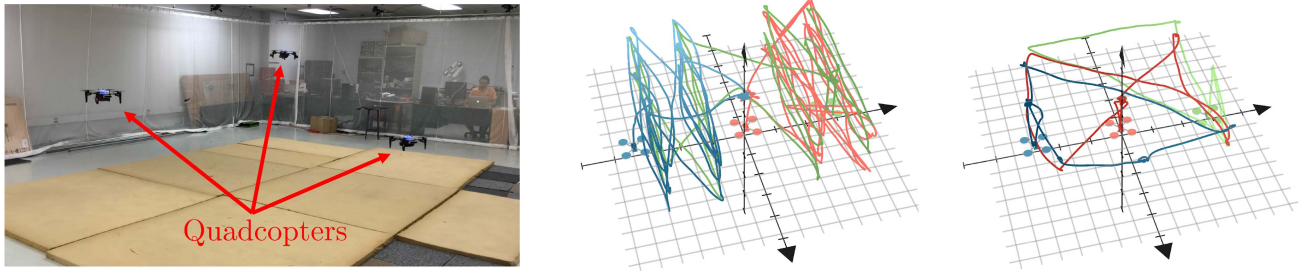


Fig. 14. (Left-hand side) In total, three quadcopters in the experimental space. (Middle) The experimental trajectory for Trial 1, where each color represents the trajectory of a different quadcopter and the grid represents a roughly $5\text{ m} \times 5\text{ m}$ area. (Right-hand side) The experimental trajectory for Trial 2.

body frame, and uses this estimate to correct the IMU measurements and inflating the covariance when constructing the RMI. In addition, each robot estimates a relative accelerometer bias to every neighbor in the robot's own body frame, which does not affect the computed RMI. For example, Robot 0's estimate of Robot i 's relative accelerometer bias is defined as

$$\beta_0^{\text{acc},0i} \triangleq \beta_0^{\text{acc},0} - C_{0i}\beta_i^{\text{acc},i}$$

where $\beta_i^{\text{acc},i}$ is Robot i 's accelerometer bias. The interested reader can refer to [48] for derivation of the pose and bias process models, corresponding linearization, preintegration, and simulation and experimental results.

B. Incomplete and Dynamic Communication Graphs

The proposed framework has been evaluated under the assumptions of a full communication graph, no packet drop, and no communication failures. Nonetheless, these are all real-world problems that must be addressed before implementing the proposed framework. This is beyond the scope of this article; nonetheless, a brief discussion regarding these issues is provided in this section.

The ranging protocol and the proposed estimator do not require a full communication graph and the lack of communication failures. However, the common-list MAC protocol does. The common-list MAC protocol is a very simple approach made possible only due to passive listening, and is ideal for small teams of robots that will always be within a communication range with one another, thus allowing a full communication graph. Whenever a ranging transaction between a pair of transceivers fails, it is reattempted multiple times until a timeout is triggered, after which the ranging pair and all other robots who have not heard a message for the duration of the timeout move onto the next entry in the list. The protocol can handle a robot's communication failure by having each robot eliminate an element in the list when it fails more than κ times, where κ is a user-defined threshold.

When extending to larger teams, it is not possible to assume that all robots are within communication range of one another, thus invalidating the full communication graph assumption. In addition, robots might fall in and out of range with one another over time, thus necessitating an incomplete dynamic communication graph model. In such scenarios, the common-list protocol is no longer simple, as robots need to know what other robots out of communication range are doing. Therefore, such

systems may benefit from other MAC protocols, such as token passing [49, Sec. 3.3], which is still possible with the proposed ranging protocol and estimator as they are independent of the choice of the MAC protocol. The benefits of passive listening thus still stand, not just due to additional measurements, but because it also allows each robot to maintain a list of neighbors within communication range.

Another implication of incomplete graphs is that each robot only estimates relative poses for the subset of robots that lie within its communication range. This is useful as it reduces the dimensionality of the onboard estimator, since each robot only estimates the relative states of $m < n$ neighboring robots. However, having dynamic graphs due to robots falling in and out of the communication range of the robot mean that the robots must initialize the states of neighbors when they appear and marginalize out the states of neighbors that have not been within the communication range for an extended period of time. The initialization can potentially be done by listening to a window of measurements from the new neighbor and formulating a least-squares problem.

XI. CONCLUSION

In this article, the problem of relative extended pose estimation has been addressed for a team of robots each equipped with UWB transceivers. A novel ranging protocol is proposed that allows neighboring robots to passively listen in on the measurements without any underlying assumptions on the hierarchy of the communication. This is, then, utilized to implement a simple MAC protocol and an efficient means for sharing preintegrated IMU information, which is then fused with the UWB measurements in a filter that estimates both the clock states of the transceivers and the relative poses of the robots. The relative poses and the preintegration are formulated directly on $SE_2(3)$. This is then all evaluated in simulation using different numbers of robots and Monte Carlo trials, and in experiments using multiple trials of three quadcopters each equipped with two UWB transceivers. The method is shown to improve the localization performance significantly when compared with centralized scenarios or to the case of no passive listening measurements.

This work can be extended to address complications that arise in wireless communication, such as packet drop. When a packet drop occurs, neighbors miss an RMI that is required to

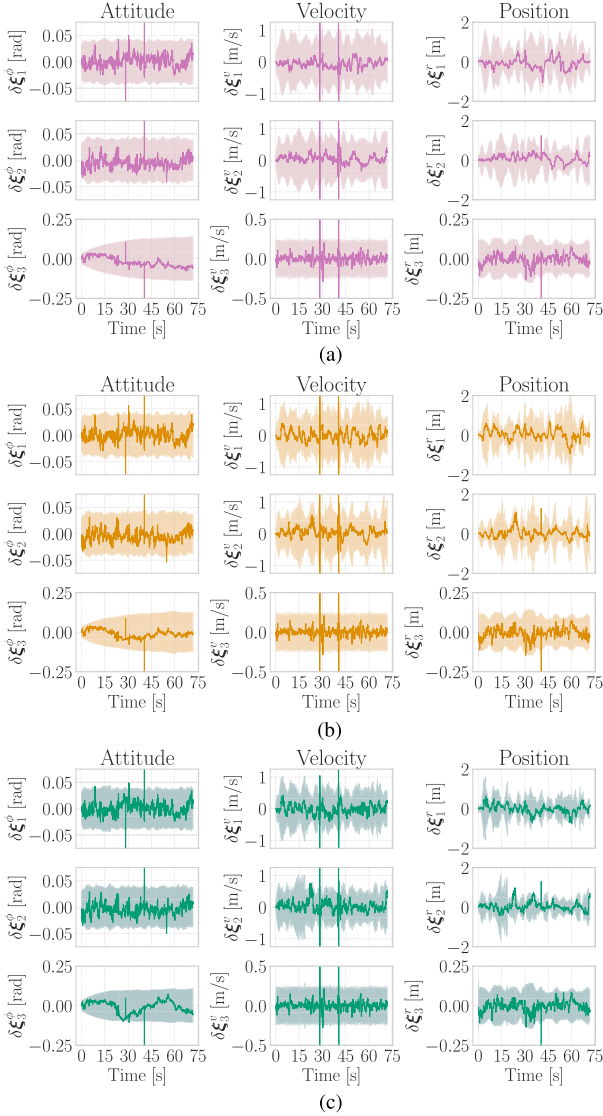


Fig. 15. Error plots and $\pm 3\sigma$ bounds (shaded region) for Robot 0's estimate of Robot 1's relative pose for experimental trial 1. (a) Centralized. (b) No passive listening. (c) With passive listening.

propagate their estimates forward, and therefore, this must be addressed in a real-world application, potentially by providing a means for robots to request a missed RMI from their neighbors. Future work will additionally consider more efficient MAC protocols where only a subset of the transceivers ranges with one another in pairs while the remaining transceivers are always passively listening. Alongside the discussion in Section X, another potential extension of this article includes collaboration between robots, as robots can share their state estimates with neighbors to reach a consensus on the clock and relative pose states.

APPENDIX A FOLD INCREASE IN MEASUREMENTS

When there are $n + 1$ robots and two transceivers per robot, the total number of transceivers is $n_t = 2(n + 1)$. Therefore, the

number of ranging pairs with transceivers on distinct robots is

$$n_p = \frac{2(n+1)(2(n+1)-1)}{2} - (n+1) = 2n(n+1).$$

The number of direct measurements between all robots is then $2n_p$ (one range and one offset measurement per pair), while the number of passive listening measurements recorded at all robots is $n_p(3(n_t - 2)) = 6nn_p$. Therefore, the fold increase in measurements is

$$\frac{2n_p + 6nn_p}{2n_p} = 1 + 3n$$

when considering a centralized approach where passive listening measurements from all robots are available.

A similar analysis can be done from the perspective of one robot that does not have access to passive listening measurements recorded at neighboring robots. Without passive listening, it can be shown that the robot only gets $8n$ distinct measurements, while with listening-in on neighboring robots' messages, the robot gets $2n_p - 8n$ new measurements from the direct measurements between the neighbors and $12n^2$ new passive listening measurements. This can be shown to be a $(\frac{1}{2} + 2n)$ -fold increase in the number of measurements from the individual robot's perspective.

APPENDIX B LINEARIZING THE RANGE MEASUREMENT MODEL

Consider as in (14) an expression of the form

$$d = \|(\mathbf{\Pi}(\mathbf{T}_2\tilde{\mathbf{r}}_2 - \mathbf{T}_1\tilde{\mathbf{r}}_1))\| \quad (47)$$

where $\mathbf{T}_1, \mathbf{T}_2 \in SE(3)$ and $\mathbf{r}_1, \mathbf{r}_2 \in \mathbb{R}^5$. Squaring both sides and perturbing the measurement and the pose states yield

$$(\bar{d} + \delta d)^2 = (\mathbf{\Pi}(\text{Exp}(\delta\xi_2)\bar{\mathbf{T}}_2\tilde{\mathbf{r}}_2 - \text{Exp}(\delta\xi_1)\bar{\mathbf{T}}_1\tilde{\mathbf{r}}_1))^T(\cdot)$$

which, using (2), can be expanded to give

$$\begin{aligned} \bar{d}^2 + 2\bar{d}\delta d \approx & (\mathbf{\Pi}\bar{\mathbf{T}}_2\tilde{\mathbf{r}}_2)^T\mathbf{\Pi}\bar{\mathbf{T}}_2\tilde{\mathbf{r}}_2 + (\mathbf{\Pi}\bar{\mathbf{T}}_1\tilde{\mathbf{r}}_1)^T\mathbf{\Pi}\bar{\mathbf{T}}_1\tilde{\mathbf{r}}_1 \\ & - (\mathbf{\Pi}\bar{\mathbf{T}}_2\tilde{\mathbf{r}}_2)^T\mathbf{\Pi}\bar{\mathbf{T}}_1\tilde{\mathbf{r}}_1 - (\mathbf{\Pi}\bar{\mathbf{T}}_1\tilde{\mathbf{r}}_1)^T\mathbf{\Pi}\bar{\mathbf{T}}_2\tilde{\mathbf{r}}_2 \\ & - (\mathbf{\Pi}\delta\xi_2^{\wedge}\bar{\mathbf{T}}_2\tilde{\mathbf{r}}_2)^T\mathbf{\Pi}\bar{\mathbf{T}}_1\tilde{\mathbf{r}}_1 - (\mathbf{\Pi}\bar{\mathbf{T}}_2\tilde{\mathbf{r}}_2)^T\mathbf{\Pi}\delta\xi_1^{\wedge}\bar{\mathbf{T}}_1\tilde{\mathbf{r}}_1 \\ & - (\mathbf{\Pi}\delta\xi_1^{\wedge}\bar{\mathbf{T}}_1\tilde{\mathbf{r}}_1)^T\mathbf{\Pi}\bar{\mathbf{T}}_2\tilde{\mathbf{r}}_2 - (\mathbf{\Pi}\bar{\mathbf{T}}_1\tilde{\mathbf{r}}_1)^T\mathbf{\Pi}\delta\xi_2^{\wedge}\bar{\mathbf{T}}_2\tilde{\mathbf{r}}_2 \end{aligned}$$

where higher order terms have been neglected. Canceling out the nominal terms on both sides, using the fact that each term is scalar, and recalling (1)

$$\begin{aligned} 2\bar{d}\delta d = & -2(\mathbf{\Pi}\bar{\mathbf{T}}_2\tilde{\mathbf{r}}_2)^T\mathbf{\Pi}\delta\xi_1^{\wedge}\bar{\mathbf{T}}_1\tilde{\mathbf{r}}_1 - 2(\mathbf{\Pi}\bar{\mathbf{T}}_1\tilde{\mathbf{r}}_1)^T\mathbf{\Pi}\delta\xi_2^{\wedge}\bar{\mathbf{T}}_2\tilde{\mathbf{r}}_2 \\ = & -2(\mathbf{\Pi}^T\mathbf{\Pi}\bar{\mathbf{T}}_2\tilde{\mathbf{r}}_2)^T(\bar{\mathbf{T}}_1\tilde{\mathbf{r}}_1)^{\odot}\delta\xi_1 \\ & - 2(\mathbf{\Pi}^T\mathbf{\Pi}\bar{\mathbf{T}}_1\tilde{\mathbf{r}}_1)^T(\bar{\mathbf{T}}_2\tilde{\mathbf{r}}_2)^{\odot}\delta\xi_2. \end{aligned}$$

Therefore, the linearized model for (47) is

$$\begin{aligned} \delta d = & -\frac{1}{\bar{d}}(\mathbf{\Pi}^T\mathbf{\Pi}\bar{\mathbf{T}}_2\tilde{\mathbf{r}}_2)^T(\bar{\mathbf{T}}_1\tilde{\mathbf{r}}_1)^{\odot}\delta\xi_1 \\ & - \frac{1}{\bar{d}}(\mathbf{\Pi}^T\mathbf{\Pi}\bar{\mathbf{T}}_1\tilde{\mathbf{r}}_1)^T(\bar{\mathbf{T}}_2\tilde{\mathbf{r}}_2)^{\odot}\delta\xi_2. \end{aligned}$$

APPENDIX C
DISCRETIZING THE INPUT MATRIX

The matrices $\tilde{\mathbf{U}}_{0,k}$ and $\tilde{\mathbf{U}}_{i,k}$ in (29) are of the general form

$$\tilde{\mathbf{U}} = \begin{bmatrix} \mathbf{u}^\wedge & \mathbf{e}_4 \\ \mathbf{0}_{1 \times 4} & 0 \end{bmatrix} \quad (48)$$

where $\mathbf{u} = [\boldsymbol{\omega}^\top \quad \boldsymbol{\alpha}^\top]^\top$, $(\cdot)^\wedge$ is the wedge operator in $SE(3)$, and $\mathbf{e}_4 = [\mathbf{0}_{1 \times 3} \quad 1]^\top$. Consequently,

$$\begin{aligned} \mathbf{U} &= \exp(\tilde{\mathbf{U}}\Delta t) = \sum_{\ell=0}^{\infty} \frac{1}{\ell!} (\tilde{\mathbf{U}}\Delta t)^\ell \\ &= \mathbf{1} + \begin{bmatrix} \mathbf{u}^\wedge & \mathbf{e}_4 \\ \mathbf{0} & 0 \end{bmatrix} \Delta t + \frac{1}{2!} \begin{bmatrix} (\mathbf{u}^\wedge)^2 & \mathbf{u}^\wedge \mathbf{e}_4 \\ \mathbf{0} & 0 \end{bmatrix} (\Delta t)^2 \\ &\quad + \frac{1}{3!} \begin{bmatrix} (\mathbf{u}^\wedge)^3 & (\mathbf{u}^\wedge)^2 \mathbf{e}_4 \\ \mathbf{0} & 0 \end{bmatrix} (\Delta t)^3 + \dots \\ &= \begin{bmatrix} \sum_{\ell=0}^{\infty} \frac{1}{\ell!} (\mathbf{u}^\wedge \Delta t)^\ell & \sum_{\ell=0}^{\infty} \frac{1}{(\ell+1)!} (\mathbf{u}^\wedge \Delta t)^\ell \mathbf{e}_4 \Delta t \\ \mathbf{0} & 1 \end{bmatrix}. \end{aligned} \quad (49)$$

Note that $\sum_{\ell=0}^{\infty} \frac{1}{\ell!} (\mathbf{u}^\wedge \Delta t)^\ell = \text{Exp}(\mathbf{u} \Delta t)$, where Exp is the $SE(3)$ exponential operator, giving

$$\sum_{\ell=0}^{\infty} \frac{1}{\ell!} (\mathbf{u}^\wedge \Delta t)^\ell = \begin{bmatrix} \text{Exp}(\boldsymbol{\omega} \Delta t) & \Delta t \mathbf{J}_l(\boldsymbol{\omega} \Delta t) \boldsymbol{\alpha} \\ \mathbf{0} & 1 \end{bmatrix}. \quad (50)$$

\mathbf{J}_l is the left Jacobian of $SO(3)$, which is of the form

$$\begin{aligned} \mathbf{J}_l(\boldsymbol{\psi}) &= \sum_{\ell=0}^{\infty} \frac{1}{(\ell+1)!} (\boldsymbol{\phi} \boldsymbol{\phi}^\times)^\ell \\ &= \frac{\sin \phi}{\phi} \mathbf{1} + \left(1 - \frac{\sin \phi}{\phi}\right) \boldsymbol{\phi} \boldsymbol{\phi}^\top + \frac{1 - \cos \phi}{\phi} \boldsymbol{\phi}^\times \end{aligned}$$

where $\phi = |\boldsymbol{\psi}|$ and $\boldsymbol{\phi} = \boldsymbol{\psi}/\phi$. Meanwhile,

$$\begin{aligned} &\sum_{\ell=0}^{\infty} \frac{1}{(\ell+1)!} (\mathbf{u}^\wedge \Delta t)^\ell \\ &= \mathbf{1} + \frac{1}{2!} \begin{bmatrix} \boldsymbol{\omega}^\times & \boldsymbol{\alpha} \\ \mathbf{0} & 0 \end{bmatrix} \Delta t + \frac{1}{3!} \begin{bmatrix} (\boldsymbol{\omega}^\times)^2 & \boldsymbol{\omega}^\times \boldsymbol{\alpha} \\ \mathbf{0} & 0 \end{bmatrix} (\Delta t)^2 \\ &\quad + \frac{1}{4!} \begin{bmatrix} (\boldsymbol{\omega}^\times)^3 & (\boldsymbol{\omega}^\times)^2 \boldsymbol{\alpha} \\ \mathbf{0} & 0 \end{bmatrix} (\Delta t)^3 + \dots \\ &= \begin{bmatrix} \sum_{\ell=0}^{\infty} \frac{1}{(\ell+1)!} (\boldsymbol{\omega}^\times \Delta t)^\ell & \sum_{\ell=0}^{\infty} \frac{1}{(\ell+2)!} (\boldsymbol{\omega}^\times \Delta t)^\ell \boldsymbol{\alpha} \Delta t \\ \mathbf{0} & 1 \end{bmatrix} \\ &= \begin{bmatrix} \mathbf{J}_l(\boldsymbol{\omega} \Delta t) & \frac{\Delta t}{2} \mathbf{N}_l(\boldsymbol{\omega} \Delta t) \boldsymbol{\alpha} \\ \mathbf{0} & 1 \end{bmatrix} \end{aligned} \quad (51)$$

where

$$\begin{aligned} \mathbf{N}(\boldsymbol{\psi}) &= 2 \sum_{\ell=0}^{\infty} \frac{1}{(\ell+2)!} (\boldsymbol{\phi} \boldsymbol{\phi}^\times)^\ell \\ &= \boldsymbol{\phi} \boldsymbol{\phi}^\top + 2 \left(\frac{1}{\phi} - \frac{\sin \phi}{\phi^2} \right) \boldsymbol{\phi}^\times + 2 \frac{\cos \phi - 1}{\phi^2} \boldsymbol{\phi}^\times \boldsymbol{\phi}^\times. \end{aligned}$$

Substituting (50) and (51) back into (49) gives

$$\mathbf{U} = \begin{bmatrix} \text{Exp}(\boldsymbol{\omega} \Delta t) & \Delta t \mathbf{J}_l(\boldsymbol{\omega} \Delta t) \boldsymbol{\alpha} & \frac{\Delta t^2}{2} \mathbf{N}_l(\boldsymbol{\omega} \Delta t) \boldsymbol{\alpha} \\ & 1 & \Delta t \\ & & 1 \end{bmatrix}.$$

REFERENCES

- [1] C. Forster, L. Carlone, F. Dellaert, and D. Scaramuzza, "On-manifold preintegration for real-time visual-inertial odometry," *IEEE Trans. Robot.*, vol. 33, no. 1, pp. 1–21, Feb. 2017.
- [2] M. Kok, J. D. Hol, and T. B. Schon, "Indoor positioning using ultrawideband and inertial measurements," *IEEE Trans. Veh. Technol.*, vol. 64, no. 4, pp. 1293–1303, Apr. 2015.
- [3] M. W. Mueller, M. Hamer, and R. D'Andrea, "Fusing ultra-wideband range measurements with accelerometers and rate gyroscopes for quadcopter state estimation," in *Proc. IEEE Int. Conf. Robot. Autom.*, 2015, pp. 1730–1736.
- [4] R. Jung and S. Weiss, "Scalable and modular ultra-wideband aided inertial navigation," in *Proc. IEEE/RSJ Int. Conf. Intell. Robots Syst.*, 2022, pp. 2423–2430.
- [5] D. Neiryneck, E. Luk, and M. McLaughlin, "An alternative double-sided two-way ranging method," in *Proc. 13th Workshop Positioning, Navigation Commun.*, 2017, pp. 1–4.
- [6] M. A. Shalaby, C. C. Cossette, J. R. Forbes, and J. Le Ny, "Calibration and uncertainty characterization for ultra-wideband two-way-ranging measurements," in *Proc. IEEE Int. Conf. Robot. Autom.*, 2023, pp. 4128–4134.
- [7] P. Groves, *Principles of GNSS, Inertial, and Multisensor Integrated Navigation Systems*, 2nd ed., Norwood, MA, USA: Artech House, 2013.
- [8] K. A. Horvath, G. Ill, and A. Milankovich, "Passive extended double-sided two-way ranging algorithm for UWB positioning," in *Proc. IEEE 9th Int. Conf. Ubiquitous Future Netw.*, 2017, pp. 482–487.
- [9] S. Shah and T. Demecheai, "Multiple simultaneous ranging in IR-UWB networks," *Sensors*, vol. 19, no. 24, pp. 1–14, 2019.
- [10] T. Laadung, S. Ulp, M. M. Alam, and Y. L. Moullec, "Novel active-passive two-way ranging protocols for UWB positioning systems," *IEEE Sensors J.*, vol. 22, no. 6, pp. 5223–5237, Mar. 2022.
- [11] A. Ledergerber, M. Hamer, and R. D'Andrea, "A robot self-localization system using one-way ultra-wideband communication," in *Proc. IEEE Int. Conf. Intell. Robots Syst.*, 2015, pp. 3131–3137.
- [12] M. Hamer and R. D'Andrea, "Self-calibrating ultra-wideband network supporting multi-robot localization," *IEEE Access*, vol. 6, pp. 22292–22304, 2018.
- [13] R. Zandian and U. Witkowski, "Robot self-localization in ultra-wideband large scale multi-node setups," in *Proc. 14th Workshop Positioning, Navigation Commun.*, 2017, pp. 1–6.
- [14] J. Cano, S. Chidami, and J. Le Ny, "A Kalman filter-based algorithm for simultaneous time synchronization and localization in UWB networks," in *Proc. Int. Conf. Robot. Autom.*, 2019, pp. 1431–1437.
- [15] A. Alanwar et al., "D-SLATS: Distributed simultaneous localization and time synchronization," in *Proc. Int. Symp. Mobile Ad Hoc Netw. Comput.*, 2017, pp. 1–10.
- [16] T. M. Nguyen, T. H. Nguyen, M. Cao, Z. Qiu, and L. Xie, "Integrated UWB-vision approach for autonomous docking of UAVs in GPS-denied environments," in *Proc. IEEE Int. Conf. Robot. Autom.*, 2019, pp. 9603–9609.
- [17] H. Xu, L. Wang, Y. Zhang, K. Qiu, and S. Shen, "Decentralized visual-inertial-UWB fusion for relative state estimation of aerial swarm," in *Proc. IEEE Int. Conf. Robot. Autom.*, 2020, pp. 8776–8782.
- [18] R. Jung and S. Weiss, "Scalable recursive distributed collaborative state estimation for aided inertial navigation," in *Proc. Int. Conf. Robot. Autom.*, 2021, pp. 1896–1902.
- [19] Q. Shi, X. Cui, S. Zhao, and M. Lu, "Sequential TOA-Based moving target localization in multi-agent networks," *IEEE Commun. Lett.*, vol. 24, no. 8, pp. 1719–1723, Aug. 2020.
- [20] M. Shalaby, C. C. Cossette, J. R. Forbes, and J. Le Ny, "Relative position estimation in multi-agent systems using attitude-coupled range measurements," *IEEE Robot. Autom. Lett.*, vol. 6, no. 3, pp. 4955–4961, Jul. 2021.
- [21] T. M. Nguyen, A. H. Zaini, C. Wang, K. Guo, and L. Xie, "Robust target-relative localization with ultra-wideband ranging and communication," in *Proc. IEEE Int. Conf. Robot. Autom.*, 2018, pp. 2312–2319.
- [22] B. Hepp, T. Nægeli, and O. Hilliges, "Omni-directional person tracking on a flying robot using occlusion-robust ultra-wideband signals," in *Proc. IEEE Int. Conf. Intell. Robots Syst.*, 2016, pp. 189–194.
- [23] Q. Shi, X. Cui, S. Zhao, S. Xu, and M. Lu, "BLAS: Broadcast relative localization and clock synchronization for dynamic dense multiagent systems," *IEEE Trans. Aerosp. Electron. Syst.*, vol. 56, no. 5, pp. 3822–3839, Oct. 2020.
- [24] Z. Dou, Z. Yao, and M. Lu, "Asynchronous collaborative localization system for large-capacity sensor networks," *IEEE Internet Things J.*, vol. 9, no. 16, pp. 15349–15361, Aug. 2022.

- [25] M. Shalaby, C. C. Cossette, J. Le Ny, and J. R. Forbes, "Cascaded filtering using the sigma point transformation," *IEEE Robot. Autom. Lett.*, vol. 6, no. 3, pp. 4758–4765, Jul. 2021.
- [26] E. Allak, R. Jung, and S. Weiss, "Covariance pre-integration for delayed measurements in multi-sensor fusion," in *Proc. IEEE Int. Conf. Intell. Robots Syst.*, 2019, pp. 6642–6649.
- [27] E. Allak, A. Barrau, R. Jung, J. Steinbrener, and S. Weiss, "Centralized-equivalent pairwise estimation with asynchronous communication constraints for two robots," in *Proc. IEEE/RSS Int. Conf. Intell. Robots Syst.*, 2022, pp. 8544–8551.
- [28] T. Lupton and S. Sukkarieh, "Visual-inertial-aided navigation for high-dynamic motion in built environments without initial conditions," *IEEE Trans. Robot.*, vol. 28, no. 1, pp. 61–76, Feb. 2012.
- [29] A. Barrau and S. Bonnabel, "Linear observed systems on groups," *Syst. Control Lett.*, no. 129, pp. 36–42, 2019.
- [30] M. Brossard, A. Barrau, P. Chauchat, and S. Bonnabel, "Associating uncertainty to extended poses for on lie group IMU preintegration with rotating Earth," *IEEE Trans. Robot.*, vol. 38, no. 2, pp. 998–1015, Apr. 2022.
- [31] J. González et al., "Mobile robot localization based on ultra-wide-band ranging: A particle filter approach," *Robot. Auton. Syst.*, vol. 57, no. 5, pp. 496–507, 2009.
- [32] R. Liu, C. Yuen, T. N. Do, D. Jiao, X. Liu, and U. X. Tan, "Cooperative relative positioning of mobile users by fusing IMU inertial and UWB ranging information," in *Proc. IEEE Int. Conf. Robot. Autom.*, 2017, pp. 5623–5629.
- [33] A. W. Long, C. K. Wolfe, M. J. Mashner, and G. S. Chirikjian, "The banana distribution is Gaussian: A localization study with exponential coordinates," *Robot.: Sci. Syst.*, vol. 8, pp. 265–272, 2013.
- [34] T. D. Barfoot, *State Estimation for Robotics, Second Edition*. Cambridge, U.K.: Cambridge Univ. Press, 2022.
- [35] LAN/MAN S. Committee, "Part 15.4: Wireless medium access control (MAC) and physical layer (PHY) specifications for low-rate wireless personal area networks (LR-WPANs)," *IEEE Comput. Soc.*, 2003.
- [36] C. C. Cossette, M. Shalaby, D. Saussié, J. R. Forbes, and J. Le Ny, "Relative position estimation between two UWB devices with IMUs," *IEEE Robot. Autom. Lett.*, vol. 6, no. 3, pp. 4313–4320, Jul. 2021.
- [37] M. A. Shalaby, C. Champagne Cossette, J. R. Forbes, and J. Le Ny, "Reducing two-way ranging variance by signal-timing optimization," *IEEE Trans. Aerosp. Electron. Syst.*, early access, 2024, doi: [10.1109/TAES.2024.3365096](https://doi.org/10.1109/TAES.2024.3365096).
- [38] A. V. Rao, *Dynamics of Particles and Rigid Bodies: A Systematic Approach*. Cambridge, U.K.: Cambridge Univ. Press, 2006.
- [39] M. Behr, P. Benner, and J. Heiland, "Solution formulas for differential Sylvester and Lyapunov equations," *Calcolo*, vol. 56, no. 4, pp. 1–33, 2019.
- [40] J. A. Farrell, *Aided Navigation: GPS With High Rate Sensors*. New York, NY, USA: McGraw-Hill, 2008.
- [41] J. Solá, J. Dera, and D. Atchuthan, "A micro Lie theory for state estimation in robotics," 2018, *arXiv:1812.01537*.
- [42] IEEE Computer Society, *IEEE Standard for Low-Rate Wireless Networks. Amendment 1: Add Alternate PHYs (IEEE Std 802.15.4a)*, IEEE Software, vol. 35, no. 2, 2018.
- [43] Decawave, "DW1000 Radio I C.," [Online]. Available: <https://www.decawave.com/product/dw1000-radio-ic/>
- [44] Y. Bar-Shalom, T. Kirubarajan, and X.-R. Li, *Estimation With Applications to Tracking and Navigation*. Hoboken, NJ, USA: Wiley, 2002.
- [45] C. C. Cossette, M. A. Shalaby, D. Saussié, J. L. Ny, and J. R. Forbes, "Optimal multi-robot formations for relative pose estimation using range measurements," in *Proc. IEEE/RSS Int. Conf. Intell. Robots Syst.*, 2022, pp. 2431–2437.
- [46] G. P. Huang, A. I. Mourikis, and S. I. Roumeliotis, "Observability-based rules for designing consistent EKF SLAM estimators," *Int. J. Robot. Res.*, vol. 29, no. 5, pp. 502–528, 2010.
- [47] G. P. Huang, N. Trawny, A. I. Mourikis, and S. I. Roumeliotis, "Observability-based consistent EKF estimators for multi-robot cooperative localization," *Auton. Robots*, vol. 30, no. 1, pp. 99–122, 2011.
- [48] M. A. Shalaby, C. C. Cossette, J. R. Forbes, and J. Le Ny, "IMU Preintegration for Multi-Robot Systems in the Presence of Bias and Communication Constraints," 2023, *arXiv:2310.08686v2*.
- [49] G. Miao, J. Zander, K. W. Sung, and S. Ben Slimane, *Fundamentals of Mobile Data Networks*. Cambridge, U.K.: Cambridge Univ. Press, 2016.



Mohammed Ayman Shalaby (Graduate Student Member, IEEE) received the B.Eng. degree in mechanical engineering in 2019 from McGill University, Montreal, QC, Canada, where he is currently working toward the Ph.D. degree in mechanical engineering.

His research interests include state estimation, multi-robot systems, and ultrawideband communication, with applications to autonomous navigation of robotic systems.



Charles Champagne Cossette (Member, IEEE) received the Ph.D. degree in mechanical engineering from McGill University, Montreal, QC, Canada, in 2023.

He is working on state estimation and planning for multirobot teams using ultrawideband radio.



Jerome Le Ny (Senior Member, IEEE) received the Ph.D. degree in aeronautics and astronautics from the Massachusetts Institute of Technology, Cambridge, MA, USA, in 2008.

From 2008 to 2012, he was a Postdoctoral Researcher with the GRASP Laboratory, University of Pennsylvania. In 2018–2019, he was an Alexander von Humboldt Fellow with the Technical University of Munich. He is currently an Associate Professor with the Department of Electrical Engineering, Polytechnique Montreal, Montreal, QC, Canada. His research interests include robust and stochastic control, mean-field control, networked control systems, dynamic resource allocation problems, privacy and security in sensor and actuator networks, with applications to autonomous multirobot systems and intelligent infrastructure systems.

Dr. Le Ny is currently an Associate Editor for IEEE TRANSACTIONS ON ROBOTICS, and a Member of GERAD, a multi-university research center on decision analysis.



James Richard Forbes (Member, IEEE) received the B.A.Sc. degree in mechanical engineering (Honors, Co-op) from the University of Waterloo, Waterloo, ON, Canada, in 2006, and the M.A.Sc. and Ph.D. degrees in aerospace science and engineering from the University of Toronto Institute for Aerospace Studies, Toronto, ON, in 2008 and 2011, respectively.

He is currently an Associate Professor and William Dawson Scholar with the Department of Mechanical Engineering, McGill University, Montreal, QC, Canada. His research interests include navigation, guidance, and control of robotic systems.

Dr. Forbes is a Member of the Centre for Intelligent Machines, a Member of the Group for Research in Decision Analysis, and a Member of the Trotter Institute for Sustainability in Engineering and Design. He was the recipient of the McGill Association of Mechanical Engineers Professor of the Year Award in 2016, the Engineering Class of 1944 Outstanding Teaching Award in 2018, and the Carrie M. Derick Award for Graduate Supervision and Teaching in 2020. He is currently an Associate Editor for the *International Journal of Robotics Research* (IJRR).